Transport, Stability, and Deposition of Gold Nanoparticles in Porous Media

Matthew Yunho Chan

Thesis submitted to the faculty of the Virginia Polytechnic Institute and State University
in partial fulfillment of the requirements for the degree of

Master of Science
In
Environmental Science and Engineering

Peter J. Vikesland
Linsey C. Marr
Mark A. Widdowson

November 15th 2011
Blacksburg, VA

Keywords: Environment, Groundwater, Gold, Nanoparticles, Engineering

Transport, Stability, and Deposition of Gold Nanoparticles in Porous Media

Matthew Yunho Chan

ABSTRACT

Gold-nanoparticle (AuNP) transport in groundwater is heavily influenced by the intrinsic properties of the nanoparticles and the external parameters of the environment. Batch experimental data indicated that 15 nm AuNP coated by bovine serum albumin (BSA-AuNP) was more stable at high ionic strength compared to citrate-coated AuNP (cit-AuNP) of similar size. It was expected that the stability of these AuNP would be replicated in column studies. Column experiments with varying monovalent and divalent ion concentrations using both types of AuNP yielded breakthrough curves that both adhere and deviate from this hypothesis. BSA-AuNP was found to be more stable relative to cit-AuNP during porous media flow in the presence of increasing concentrations of $CaCl_2$, but the opposite occurred with increasing NaCl concentration. Colloidal filtration theory (CFT) fails to predict and explain this discrepancy. DLVO calculations suggested pore-space destabilization occurred in these experiments that were not accounted by CFT.

Acknowledgement

This project would not be possible without the guidance and leadership from my committee members: Dr. Linsey Marr, Dr. Mark Widdowson, and my research advisor Dr. Peter Vikesland, my most sincere thanks for their wisdom and their generosity in sharing that wisdom. I would also like to thank all the members of the Vikesland group, especially my coauthors on the manuscript I am preparing for publication, Dr. Matt Hull and Jason Jones; none of these intriguing results would have been possible without the input and hard works you have provided. The rest of the Vikesland group: Becky Halvorson, Ron Kent, Param Pati, Dr. Xiaojun Chang, Dr. Weinan Leng, Dr. Rob Rebodos, Dr. Matt Fiss, Bryan Sinclair, Dr. Andy Whelton; as well as other members of the VTSuN group: Carol Johnson, Dr. Rebecca French, Nina Quadros, Andrea Tiwari, Dr. Amara Holder, Dr. Beth Diesel, and others; your support and friendship sustained me through difficult parts of this project. Special thanks must be given to Shihong Lin at Duke Univeristy for his help in setting up the experiment. I would also like to take this opportunity to acknowledge the funding agency of this project, the Center for the Environmental Implication of NanoTechnology; a research center jointly funded by the National Science Foundation and the Environmental Protection Agency. I would also thank the Virginia Tech Institute for Critical Technology and Applied Science for providing excellent and state of the art lab space. Many thanks must be given to Betty Wingate, Beth Lucas, Jody Smiley, and Julie Petruska for support from the Charles E. Via, Jr. Department of Civil and Environmental Engineering. And finally, I would like to thank my friends and family, who supported me during my darkest time, and reaffirming my faith in things that mattered. Thank you, with all my heart.

Table of Contents

Table of Figures

Table of Figures (Tables)

Chapter 1 – Introduction

The application of nanomaterials by industry and their use in consumer products is becoming increasingly popular each year. The U.S. National Nanotechnology Initiative (which includes government agencies such as the NSF, NIH and EPA) provided as much as $849 million for nanotechnology research funding in the 2004 fiscal year.[1] Consumer products containing nanomaterials experienced a 521% growth between 2006 and 2011.[2] Nanotechnology's attraction to researchers, industry and consumers stems from the fact that nanomaterials feature novel and unique properties not found in macroscopic materials.[3,4] The novel features that nanomaterials exhibit are wide ranging and can include electronic, optical, thermal, and photoactive properties.[4,5]

In particular, gold nanoparticles (AuNP) show very promising potential applications in many different fields. In the biomedical industry, AuNP show great promise in the field of drug delivery to target specific regions in the body that are usually difficult to reach.[6] There has been much work investigating the possibility of applying AuNP as a tumor treating vector.[7–10] AuNP also display great potential in the material science industry. Self-assembling conductive films have been successfully produced and characterized, and are potentially revolutionary in the production of new microelectronic products.[11] Further application of this self-assembling property of AuNP has shown that thin gold sensor films can be produced for vapor sensing applications.[12] In the field of chemistry, AuNP was found to exhibit low-temperature catalytic abilities; enabling many applications for consumers such as indoor air quality control and pollutant emission control.[13] In analytical chemistry, AuNP is used in surface enhanced

Raman spectroscopy, which can detect trace substances down to the femtogram scale.[14]

While all these new prospects of technological application are very exciting, there is a hidden danger. Production of nanomaterials, and specially manufactured nanoparticles have increased year after year.[15] There are currently little to no regulations governing the release and disposal of these materials.[16] Therefore, it is of little doubt that the release of nanomaterials, for example, AuNP, is occurring right now, and will only increase with time. AuNPs that are released can be potentially transported throughout the environment. Depending on their final destination, AuNPs can partition to the aqueous/marine food web, or to the terrestrial food chain.[17,18] There is evidence that AuNP, once consumed by living organisms can readily partition into their cells.[19] Preliminary toxicological studies reveal that AuNP potentially exhibit cytotoxicity (that is, toxicity to cells).[20] Hence, it is very important for gold nanoparticles' fate and transport behavior to be fully understood, especially in a complex system such as a groundwater aquifer.

Before the field of study that is nanotechnology became prominent, colloidal material encompassed the size range where suspended solids were considered nanomaterials (< 100 nm).[21] Therefore, the study of nanoparticle through groundwater usually starts with treating them as classical colloidal materials. When a colloidal material is released into porous media, such as the groundwater environment, many possibilities exist. If the chemistry of the pore water and the porous media allow the nanoparticle to remain stably suspended in the pore water, then it is possible that the

particles will not be retained within the aquifer, and eventually will be transported out of the groundwater system.[22] However, often-times the properties of the environment will induce instability in the nanoparticle suspension. The attractive force from van der Waals interactions and the repulsive force from electrostatic interactions between the solids in the groundwater system govern the stability of the nanoparticles.[22] The nanoparticles can interact physiochemically with the surface of the porous media, where the particles are immobilized and deposited within the pore space of the aquifer. The nanoparticles themselves can also attract one another, resulting in a size growth due to aggregation. These nanoparticle aggregates can become so large that they are physically strained or filtered by the pore space of the aquifer, thus removing them from the flow. In reality, the transport behavior of nanoparticles will be a combination of all these possibilities, dictated by the surface chemistry of the nanoparticles and porous media, the solution chemistry of the pore water, and other external factors in the environment.

Nanoparticle Transport in Porous Media. There are several effective laboratory methods to simulate and investigate nanoparticle transport through porous media. A popular method is to utilize a packed column. This method is similar to column chromatography, where an inflow containing the desired analyte is passed through a column packed with a porous medium. The analyte interacts with the media within the column, then elutes out of the other end. However, column chromatography is usually employed as a separation method; due to the chemistry and physics of the media different components of the analyte pass through the column at different velocities, thus achieving separation. The purpose of a packed column experiment for nanoparticle

transport analysis is different. Here, the packed column is designed as a one-dimensional representation of a groundwater environment. By analyzing and comparing the chemistry between the inflow and outflow, important information regarding the transport behavior and stability of nanoparticles in porous media can be obtained.

Another popular method is to use a quartz crystal microbalance (QCM). The QCM consists of a piezoelectric quartz crystal that exhibits a very specific resonance frequency when an electrical current is applied to it. This resonance frequency is very sensitive to the magnitude of any external mass adhering to the crystal.[23] This property can be exploited to investigate solid deposition from the aqueous phase.[24] Similar to the packed column method, a flowing solution containing nanoparticles passes across the QCM. The surface of the QCM can be modified to mimic surfaces in the environment.[25] When the nanoparticles in the flow interact with the QCM, leading to deposition onto the microbalance surface, the instrument will detect a change in the resonance frequency. The frequency change can be analyzed and related to the deposition behavior of the nanoparticles. The QCM method is popular because of its superior sensitivity. However, QCM is not necessarily a better method than a packed column experiment. The crystal in a QCM is usually a flat surface (or the radius of curvature is so large compared to that of a nanoparticle that it essentially behaves like a flat surface) and thus it lacks any curvature a sediment particle in nature would have. This difference in curvature will alter how adhering matter interacts with the surface of the QCM.

There are also other less commonly used methods to analyze nanoparticle fate and transport. A method that is gaining popularity is to use a two-dimensional structure as the porous medium. Usually, this is done by fabricating glass wafers via

photolithography and chemical etching.[26] This 2D method is similar to the packed column method, except in the column case, flow was only considered in one-dimensional space. The advantage of constraining flow to one-dimension is that the governing boundary condition becomes much simpler. The disadvantage is that it is not a complete representation of what actually occurs in the environment (three-dimensional flow). By using a porous media that promotes two-dimensional flow, the results from the experiment may be more reflective to what actually happens in nature. The difficulty for the two-dimensional flow method arises with the calculations. Often times the math becomes very complicated and unwieldy for efficient analysis.[26]

Colloid Filtration Theory. Because of its general robustness and ease of use, the packed column method was chosen as the primary experimental method for this work. The primary output data from a column experiment is a breakthrough curve. A breakthrough curve is a plot of the concentration of nanoparticles in the column outflow versus time (often represented in terms of pore volumes, which is the amount of time required for the flow to completely fill up the pore space of the column). A breakthrough curve is raw data that contains a significant quantity of information that can be further analyzed. A common method is to apply colloid filtration theory to the data.

In colloid filtration theory, a grain of porous media (silica beads, sand, sediment or other aquifer material) can be classified as a collector.[27] Nanoparticles that are flowing near a collector can come into contact with the collector surface by several mechanisms. On occasion, the size of the nanoparticles may become big enough that the fluid flow-lines transporting the nanoparticles are close enough to the surface that the particles make contact with the collector. This process is classified as interception.

On the other hand, if the nanoparticle density is sufficiently high that it is affected by gravity, sedimentation can enable contact between the nanoparticles and the collectors. Because nanoparticles are quite small, their Brownian motion will be significant.[3] The contribution of Brownian diffusion to the contact between nanoparticles and collectors is thus often very significant.[3] The single-collector efficiency (η_0) combines all three contributions to yield a ratio between the rate at which particles make contact with the collectors and the rate at which particles flow towards the collector.[28]

$$\eta_0 = \eta_D + \eta_I + \eta_G \quad (1)$$

In equation (1), η_D is the Brownian diffusion contribution to the single-collection efficiency, while η_I and η_G are the interception and sedimentation contribution respectively. Numerous researchers have modeled each of these terms differently, but Tufenkji and Elimenech developed a robust form in 2004.[28] According to them, each of the terms are defined as such:

$$\eta_D = 2.4A_S^{1/3}N_R^{-0.081}N_{Pe}^{-0.715}N_{vdW}^{-0.052} \quad (2)$$

For the diffusion term, A_s is a parameter based on porosity; N_R is a parameter that describes the dimension of the nanoparticles and the collectors; N_{Pe} is the Péclet number, which is the ratio between advective and diffusive contribution to the flow, and N_{vdW} is a parameter describing van der Waals interaction between collectors and nanoparticles and is based on the Hamaker constants of either material.

$$\eta_I = 0.55A_SN_R^{1.675}N_A^{0.125} \quad (3)$$

For the interception term, A_s and N_R are defined the same way as mentioned above. N_A is the attraction number, which is a function of the velocity and viscosity of the fluid, as well as the size of the nanoparticles.

$$\eta_G = 20.22 N_R^{-0.24} N_G^{1.11} N_{vdW}^{0.053} \quad (4)$$

Finally, the sedimentation term is also defined by N_R and N_{vdW} which were defined above, as well as N_G, which is the gravity number, a function of viscosity and velocity of the fluid, as well as the size and density of the nanoparticles. The combined single-collector efficiency (η_0) is a very important parameter for column experiments, as it governs the probability of collision between a nanoparticle and a grain of media in the column.

Once contact has been made between a nanoparticle and a collector surface the physiochemical properties of both bodies determines whether or not nanoparticle attachment occurs. The probability of attachment is difficult to determine theoretically, which is why empirical data from column experiments are needed. By analyzing the breakthrough curves (output data from the column experiments), and combining them with the single-cell collector efficiency, the attachment efficiency (α) can be determined. The attachment efficiency is defined as the ratio of the rate of particle attachment onto a collector and the rate of particle collision with a collector.[29] The calculation of α requires input of empirical data (in the form of C/C_0, i.e., concentration of particles in outflow normalized by concentration of particles in inflow) as well as η_0.

$$\alpha = -\ln\left(\frac{C}{C_0}\right)\frac{(4a_c)}{3(1-\epsilon)\eta_0 L} \quad (5)$$

Additional parameters required for α calculations are a_c, radius of the collector; ϵ, porosity of the packed column, and L, the length of the column. The understanding of nanoparticle transport and fate is invaluable as it describes immobilization and deposition process of particles that is due to due to interception, gravitational sedimentation, and Brownian diffusion.

DLVO Theory. Although the attachment efficiency as an empirical coefficient usually describes the interaction between nanoparticles and porous media adequately, it relies heavily on the quality of the empirical data. Classically particle interactions in aqueous environments have been evaluated using the Derjaguin – Landau – Verwey – Overbeek theory (DLVO). DLVO theory essentially states that colloidal particle stability (i.e., the ability to remain dispersed in an aqueous medium) is governed by the balance between van der Waals interactions (i.e., interaction of dipoles) and the force of electrostatic interactions (i.e., forces between the electronic double layer present at the particle surfaces).[30,31] DLVO theory maintains that the sum of these two interaction energies is a function of distance between the two interacting particles (which can be either both nanoparticles, or a nanoparticle and a grain of porous media) and dictates whether attractive or repulsive forces dominate. As two surfaces approach one another, they initially exhibit a sum of negative interaction energy, which manifests as a relatively weak attractive interaction between the two surfaces (Figure 1). This attractive interaction is called the attractive secondary minimum. As the surfaces move closer and closer to each other, repulsive forces begin to dominate, cumulating in a repulsive energy (positive) energy barrier. However, if for whatever reason the two surfaces continue to move closer together, the sum of interaction energy will eventually exhibit a

rapid and sudden shift towards a very favorable attractive dominance (very strong negative energy) called the attractive primary minimum.

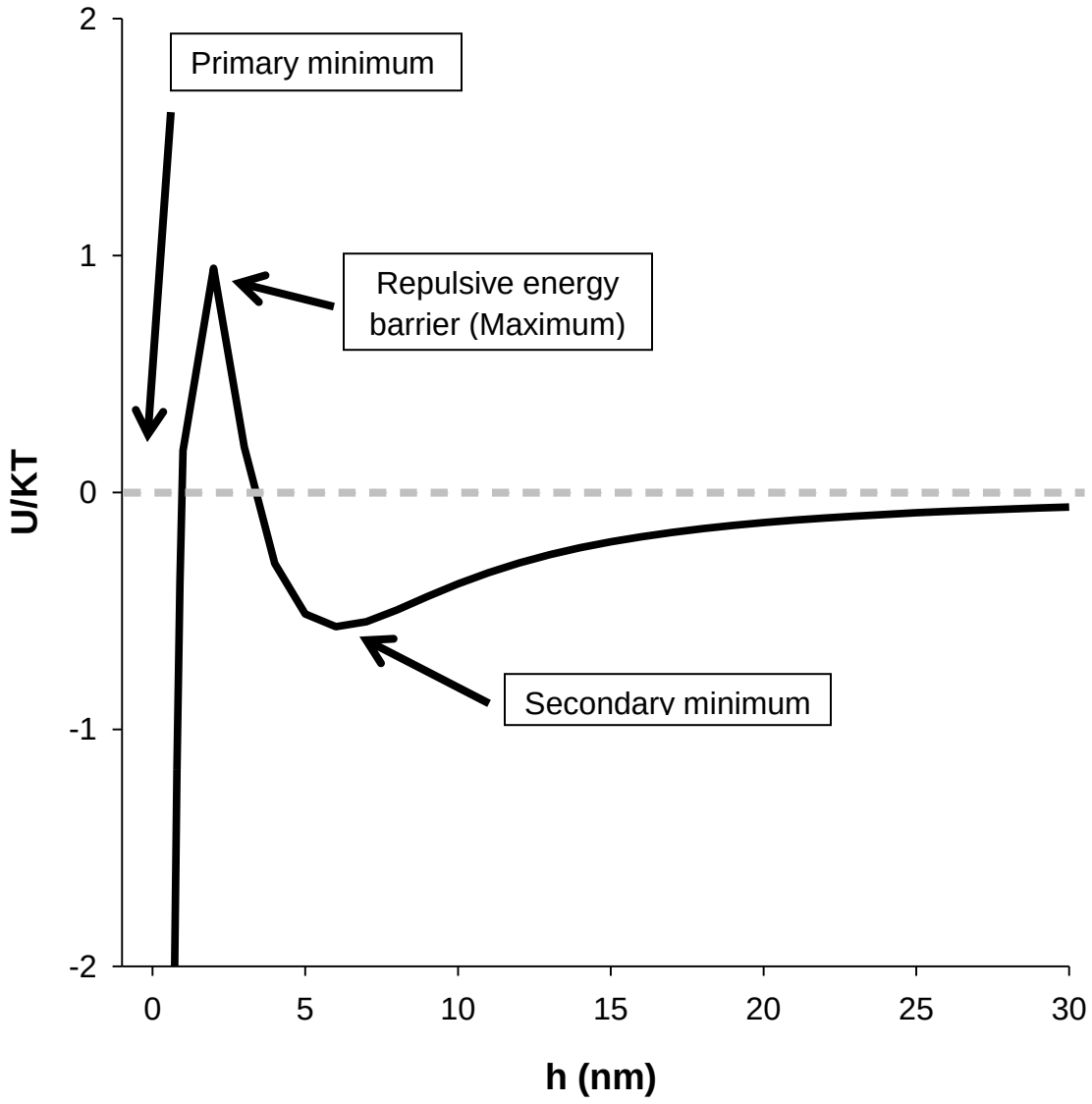

Figure 1 – A typical DLVO curve. The x-axis h is the distance between two surfaces in nanometers. The y-axis gives the dimensionless energy expression (energy divided by K – the Boltzmann constant and T – the absolute temperature). Note the attractive secondary minimum at ~6 nm, the repulsive maximum at ~3 nm and the primary minimum well.

DLVO calculations are mostly theoretical and require no empirical data (it only needs environmental parameters), and are thus able to account for interactions not covered by colloid filtration theory. Combining these two theoretical frameworks, along with

experimental results will give rise to a much better understanding of AuNP fate and transport in a porous media.

Previous Column Transport Studies. Column experiments have been heavily utilized by others to investigate the fate and transport of many different kinds of nanomaterials. Lecoanet and Wiesner utilized a column experiment to study the effects of flow velocity to nanoparticle transport in porous media.[32] The porous media used by Lecoanet and Wiesner was homogeneous micron sized glass beads and the nanoparticles investigated were primarily fullerenes and fullerene oxides. The breakthrough curves from the column experiments became increasingly irregular as the flow rate increased. Lecoanet and Wiesner noted that as they increased flow velocity that the level of nanoparticle removal converged to a point that was independent of the velocity. They also observed an unusual dip during the initial slope of the breakthrough curve, which they attributed to a change in deposition mechanism from physiochemical interaction between the surfaces to physical straining of the nanoparticles. This dip was, however, only observed the very high velocities and has not been replicated by others. The transport of nC_{60} (a representative fullerene) was also examined by Espinasse *et al.*, where they attempted to identify external factors that may affect the degree of nanoparticle retention. By using column experiments, DLVO theory, and colloidal filtration theory ($\eta_0$and α) as described above, they arrived at the conclusion that high ionic strengths, the presence of polysaccharide-type organic matter and low flow velocities tend to correlate with high fullerene retention in the column.[33]

There are occasionally conflicting results from nanoparticles column experiments, especially when comparing column based experimental results to theoretical results

calculated via DLVO. For example, in a series of nC_{60} experiments, Wang *et al.* reported that the transport and deposition of the nC_{60} nanoparticles was accurately simulated by a DLVO derived mathematical model, as they agreed with empirical data obtained from a column packed with glass beads, as well as with sand.[34] However, in a similar study by Li *et al*., they compared theoretically and empirically determined collector efficiency (η_0) values and found that they were off by one order of magnitude.[35] While this type of discrepancy has been seldom reported, it may be an indication that classic DLVO theory and colloidal filtration theory may need to be modified to account for nanoparticle transport in porous media.

The fate and transport of polymer nanoparticles such as latex spheres have also been extensively investigated. Franchi and O'Melia utilized a glass bead packed column for their latex nanoparticle experiments.[36] The nanoparticles used in these experiments were 98 nm in diameter. In their experiments, they noticed that certain nanoparticles exhibit what is called reentrainment, which is the detachment of nanoparticles that were previously immobilized by a collector (in this case, a glass bead). It was determined that in the presence of macromolecules such as humic acid, the reentrainment behavior increased, probably due to steric and electrostatic contributions to the repulsive interaction between the latex nanoparticles and the collectors. Reentrainment was possible due to what is known as secondary minima deposition. Recall that in the energy plot of DLVO theory, there exists a small minimum in total interaction energy before the repulsive maximum (see Figure 1). It is possible that nanoparticles were deposited at this secondary energy minimum, where escape from the attractive interaction was relatively easy. Franchi and O'Melia noted that at lower ionic strength,

attachment of nanoparticles to the collectors was relatively reversible as it primarily occurred at the secondary energy minimum. At higher ionic strengths, the deposition mechanism shifts to irreversible capture in the primary DLVO energy well. This result was confirmed by a separate study performed by Tufenkji *&* Elimelech (again with latex nanoparticles and glass beads).[37] In their experiments, they utilized numerous methods to eliminate the possibility of secondary minima deposition. It was found that when it was only possible to deposit nanoparticles at the primary energy well, the resulted calculated parameters agreed much more consistently with colloid filtration theory.[37] Further discrepancies between theoretical predictions and empirical results were observed in yet another study of latex nanoparticles. Pelley and Tufenkji reported in their experimental results that at low ionic strength α increases with particle size, which was not what DLVO theory predicted.[38]

Other types of nanomaterials have been investigated in the same way as well. Saleh *et al.* examined zero valent iron nanoparticles that were surface modified.[39] The surface modifiers encompassed a wide range of molecular weights. However, it was determined that while most of the modifiers provided electrostatic stabilization to the nanoparticles, it was a polymer coating that provided electrosteric stabilization that enabled the greatest mobility of the nanoparticles through the porous media. Studies involving carbon nanotubes were proven to be unique due to the nanotubes non-spherical morphology. In a study by Jaisi *et al.*, this non-spherical contribution was confirmed as they found that during a column experiment with a pure water mobile phase that a relatively low breakthrough was observed.[40] They attributed this finings are the result of the very large aspect ratio of the nanotubes, large amount of physical

straining were occurring inside the column.[40] This theory of aspect ratio contribution to deposition mechanism was affirmed in a subsequent study by Jaisi and Elimelech.[41] Here they compared column experiment results between carbon nanotubes and nC_{60}. They found that experiments involving nC_{60} were much more sensitive to ionic strength changes than those involving nanotubes.[41] Jaisi & Elimenech concluded that the shape of the nanotube made physical filtration a much more favorable removal mechanism.[41]

It is important to note that the numerous column studies mentioned previously all have a common factor. As Petosa *et al*. have indicated, all α values obtained from the column study approach 1 as the environment was changed to favor deposition.[5] One of the rare occasions when α was far from 1 even when large amounts of nanoparticles were removed by the column was a study done by Solovitch *et al.* with TiO_2 nanoparticles.[42] In their study, it was found that even though the breakthrough curves indicated that a large amount of nanoparticles were removed in some condition, α was still extremely small. This result was not observed by others. Solovitch *et al*. attributed this finding to the possibility that the nanoparticles were concurrently aggregating and depositing, and that the α values fail to take into account this process. All these column studies point to the fact that while there are many occasions that DLVO theory and colloid filtration theory could successfully predict fate and transport behavior of nanoparticles, there are still significant instances where major discrepancies occur.

For the experiments performed in this work, similar column experiments as performed by many others were repeated. However, the nanoparticle in question was gold nanoparticles. As described above, gold nanoparticles have many important

applications in many industries. It is prudent to understand their as yet unknown fate, stability and transport behavior in aqueous porous media. In addition, the work presented here also seeks to compare and contrast the fate and transport of AuNP with different surface functionalization. The surface of AuNP is typically coated with a stabilizer to prevent aggregation; oftentimes this will be citrate as it is used as the primary reducing agent during synthesis.[43] In biomedical applications, AuNP is often further coated with proteins such as bovine serum albumin (BSA).[44] As mentioned by Saleh *et al.*, surface modifications of nanoparticles by these larger macromolecules will result in more stabilized particle suspensions.[45] Therefore, the hypothesis for the presented study was that in the column experiments, BSA functionalized AuNP (BSA-cit-AuNP) will have a higher mobility and be more resistant to ionic strength changes when compared to AuNP that are only stabilized by citrate (cit-AuNP).

Chapter 2 – Materials and Methods

Unless specified otherwise, all water used in these experiments was ultrapure with a resistivity of 18.2 MΩ·cm (Barnstead Nanopure, Thermo Scientific; Asheville, NC). All glassware was cleaned using a laboratory glassware disinfector-washer (Lancer 1400 LXP, Lancer Industry; Winter Springs, FL), utilizing a proprietary mixture of non-foaming detergent (a strong base and oxidizer) and a non-foaming neutralizing acid to thoroughly clean glassware. All glassware that was in contact with AuNP suspension was additionally pre-cleaned with Aqua Regia to ensure complete removal of remnant gold. Prior to use, the glassware was copiously rinsed with ultrapure water.

Preparation of the porous media. Spherical soda-lime glass beads (MO-SCI; Rolla, MO) were used as the porous media in the column experiments. According to the manufacturer the average size of these beads was 260 μm and as described herein this size was corroborated by SEM imaging. Prior to use, the beads were extensively washed using the method of Tufenkji *et al*.[46] Briefly, the beads were cleaned by soaking in a 2% Extran® MA02 detergent solution (EMD Chemicals; Gibbstown NJ) for 1 hour, followed by a thorough rinse with reverse osmosis (RO) treated water. The beads were then sonicated in 2% RBS 25 detergent solution (Pierce; Rockford IL) for 1 hour, and again rinsed with RO water. The beads were then soaked for 24 hours in a sulfuric acid (Fisher Scientific; Fair Lawn, NJ) activated glass cleaning solution (NOCHROMIX®, GODAX Laboratories; Cabin John, MD). Following these cleaning steps, the beads were rinsed with RO water until the pH of the rinse effluent was ≈5.6. The beads were then dried overnight in an oven at 80 ^{o}C. Prior to use, the cleaned beads were stored in a vacuum desiccator.

Porous media characterization. The glass beads utilized as the porous media in the packed column were characterized for their electrostatic properties. Streaming potential measurements were performed on a ≈2 g sample of the glass beads using an electrokinetic analyzer (SurPASS, Anton Paar, Ashland, VA). Three titration curves were obtained in a 2 mM $NaHCO_3$ solution. The three titrations differed with respect to their mobile phase electrolyte content. These electrolytes were 10 mM NaCl, 1 mM $CaCl_2$ and a blank that contained only the bicarbonate buffer. Titrations were conducted from pH 9 to pH 5 by utilizing a 0.2 M NaOH titrant. The measured streaming potential was converted into zeta potentials by the on-board software via a modified form of the Helmholtz-Smoluchowski equation.[47]

Gold nanoparticle synthesis. Citrate-coated gold nanoparticles (cit-AuNP) of ≈15 nm diameter were prepared as described by Turkevich.[43] In this production protocol, citrate act as both a reducing agent and as a surface stabilizer.[48] All suspensions were filtered (0.2 μm sterile vacuum filter), transferred to a glass vial, and stored in the dark at 4 ^{o}C until use. Bovine serum albumin-coated cit-AuNP (BSA-cit-AuNP) were prepared by incubating cit-AuNP with 0.1 mg/mL BSA as described by Ao *et al*.[49] All suspensions were sterile-filtered (0.2 μm), and stored in the dark at 4 ^{o}C.

AuNP Characterization. Both types of AuNP were analyzed by transmission electron microscopy (TEM). A Zeiss 10CA TEM equipped with a high resolution (1024 × 1024 pixel) MT Advantage GR/HR-B CCD Camera System (Advance Microscopy Techniques Corp.; Woburn, MA) with an accelerating voltage of 60 kV was used to characterize AuNP size and morphology. Aliquots of 10 – 20 μL of either type of AuNP

suspension were transferred onto a carbon-coated copper TEM grid (Electron Microscopy Sciences; Hatfield, PA). Once completely dried, the TEM grid was placed into the microscope for analysis. Micrographs were analyzed using ImagePro (MediaCybernetics; Bethesda, MD) to determine the AuNP core size.

The electrostatic properties of AuNP were measured using a particle analyzer (Zetasizer Nano ZS, Malvern; Westborough, MA) equipped with an autotitrator (MPT-2, Malvern). Cit-AuNP and BSA-cit-AuNP suspensions in 2 mM $NaHCO_3$ (pH≈8.2) were each titrated by NaCl (0 – 60 mM) and $CaCl_2$ (0 – 1 mM), resulting in four titration curves. The particle analyzer was also used to obtain dynamic light scattering (DLS) measurements of the particle size distributions for both types of AuNP suspensions.

Once a given AuNP suspension was synthesized, the total gold concentration was measured by inductively coupled plasma mass spectrometry (X-Series ICP-MS, Thermo Scientific; West Palm Beach, FL). A 1 mL aliquot of AuNP suspension was dissolved in 2 µL of Aqua Regia and the resulting ionic gold solution was analyzed by ICP-MS according to AWWA Standard Methods 3125 B.[50] The concentration of the stock AuNP suspension used for the column experiments was ≈160 mg/L. After dilution (procedure described below) during the column experiment injection, the initial concentration of AuNP entering the column was ≈24.5 mg/L.

UV-Vis spectroscopy was used to quantify the gold nanoparticle concentration. Calibration curves plotting the intensity of the absorbance maximum of the localized-surface plasmon resonance (LSPR) band for AuNP (520 nm for cit-AuNP and 526 nm for BSA-cit-AuNP) as a function of gold nanoparticle concentration were obtained each

time a column experiment was performed. The extinction coefficients obtained over the course of multiple calibration curves raged from 0.0179 to 0.0219 ($\bar{x} = 0.01945, n = 33, s_N = 9.33 \times 10^{-4}$). The extinction coefficients from the calibration curves have a very narrow range and a very small standard deviation (s_N).

Batch experiments. Batch experiments were conducted to examine the affinity between cit-AuNP and the porous media in the absence of flow. Using a series of 50 mL Erlenmeyer flasks, 20 mL of a ≈30 mg/L AuNP suspension was added to each flask. In addition, 5 g of the cleaned glass beads were placed into the flask containing the AuNP. Solution pH was adjusted from 5 to 9 via HCl and NaOH addition and the ionic strength was adjusted from 0.1 to 50 mM with NaCl. These flasks were sealed tightly with parafilm and then placed onto a rotary shaker for a period of three days. Over the course of the experiment, 2 mL aliquots of supernatant were removed every 24 hr and analyzed via UV-Vis spectroscopy. By subtracting the detected AuNP concentration in the supernatant from the initial AuNP concentration the amount of AuNP attached to the porous media was obtained.

Column experiments. Column experiments were performed using a glass column with an inner diameter of 0.16 cm and a maximum length of 20 cm (C 10/20, GE Healthcare; Piscataway, NJ). An adjustable plunger facilitated adjustment of the length of the porous media bed. For all experiments described herein, however, the active (packed) column length was fixed at 10 cm. The column was dry packed with periodic tapping of the added, treated glass beads to a 10 cm depth. The total pore volume and porosity of the column were determined by comparing the dry weight of the packed column to the weight of a water filled (but no porous media) column. Pore volume (V_{pore})

and porosity were carefully adjusted to 7.05 mL and 34% each time an experiment was performed. Once the porous media was secured in the column, a mobile phase of 2 mM $NaHCO_3$ was introduced into the packed column at high flow (≈ 30 mL/min). When the packed column was fully saturated, the flow was decreased to the experimental flow rate, and the column was then equilibrated with the mobile phase flow for a minimum of 10 addition pore volumes.

The flow system consisted of two syringe pumps connected in parallel. A large volume syringe pump (Model 500D, Teladyne ISCO; Lincoln, NE) was used to supply the mobile phase, while a smaller pump (PHD2000, Harvard Apparatus; Holliston MA) was used to inject the AuNP suspension (Figure 2). All components of the flow system were connected using PTFE tubing of either 1/16 or 1/32 inner diameter. Initial attempts to use stainless steel tubing failed due to AuNP retention within the tubing. The flow rate of the mobile phase was 2.413 mL/min and the AuNP injection rate was 0.43 mL/min. During injection, a valve was engaged to introduce the AuNP suspension into a mixing tee, where turbulent mixing with the mobile phase occurred. In most experiments a five pore volume injection volume and a 7.5 min injection time were used. Once the injection volume goal was reached, the valve was switched and a second syringe containing only mobile phase was injected for the remainder of the experiment. In this manner, the flow through the column was continually maintained at 2.843 mL/min (i.e., a Darcy velocity of 0.023 cm/s) regardless of whether or not AuNP were being injected. The effluent from the column entered into a quartz flow-through cell (Starna; Atascadero CA) for analysis by UV-Vis spectroscopy. The mobile phase had a varying ionic strength depending upon the experiment. Monovalent salt concentrations in the mobile phase varied from

10 – 70 mM NaCl (Fisher Scientific; Pittsburgh, PA), while the divalent salt concentration was varied from 0.1 – 0.6 mM $CaCl_2$ in parallel experiments (Fisher Scientific; Pittsburgh, PA). Each set of experiments varying the ionic strength were performed using cit-AuNP and BSA-cit-AuNP.

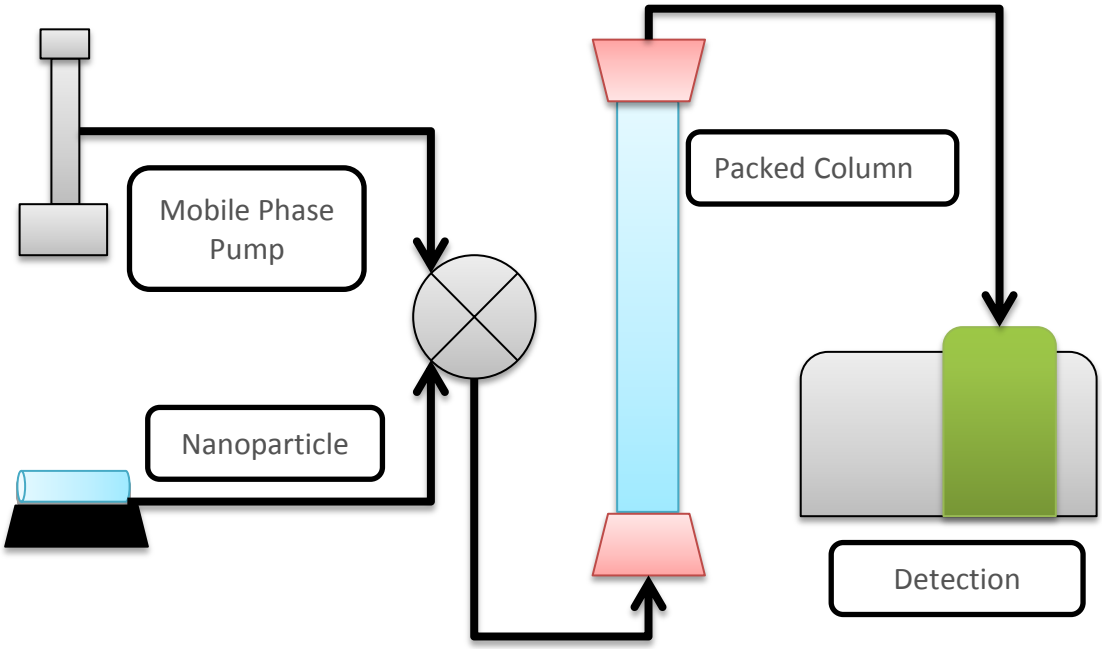

Figure 2 - Column experiment setup schematic

Prior to and after each AuNP injection experiment, an inert $NaNO_3$ solution was injected into the column as a tracer. All experimental parameters remained the same. The nitrate tracer provided hydrodynamic information about the column, while comparison of the two tracer data sets (before and after AuNP injection) provides a qualitative internal standard and serves to illustrate whether any changes occurred to

the porous media during the experiment. The nitrate concentration was evaluated by the spectrometer at 302 nm.

Chapter 3 – Results and Discussion

Nanoparticle and Porous Media Characterization. The cit-AuNP and BSA-cit-AuNP nanoparticles used in this study were characterized with respect to their morphology and surface charge. As shown in Figure S1, both nanoparticle types are highly monodisperse. Cit-AuNP and cit-BSA-AuNP both have core diameters (d_{TEM}) of 15 $\pm$ 6.8 nm (n=619 for cit-AuNP) as determined via image analysis of the collected TEM images. The d_{TEM} values were corroborated by dynamic light scattering (DLS) measurements that indicate hydrodynamic diameters (d_{DLS}) of 19.7 ± 0.1 for cit-AuNP and 29.4 ± 0.1 for BSA-cit-AuNP. The increase in d_{DLS} for BSA-cit-AuNP relative to cit-AuNP is consistent with the existence of a BSA over-layer surrounding the nanoparticles. In addition, the larger value for d_{DLS} relative to d_{TEM} for cit-AuNP was expected due to the presence of a surface hydration layer that could not be detected by TEM imaging.

Electrophoretic mobility measurements were obtained to evaluate the surface charge of cit-AuNP and BSA-cit-AuNP under conditions representative of those used in the deposition studies. As summarized in Table 1, the electrophoretic mobility values for cit-AuNP and BSA-cit-AuNP were -2.05 ± 0.13 and -1.95 ± 0.19 (with units of $\mu m \cdot cm \cdot V^{-1} \cdot s^{-1}$). The corresponding zeta potentials for cit-AuNP and BSA-cit-AuNP were -38.4 ± 1.00 mV and -24.6± 1.64 mV respectively. The Smoluchowski equation enabling the calculation of zeta potential from the raw electrophoretic mobility data is valid for cit-AuNP.[51] However, it is questionable whether such a calculation is appropriate for protein coated BSA-cit-AuNP. Nonetheless, the calculated zeta potential values are reported

here for consistency with the literature. The decrease in the apparent surface charge following the association of BSA is consistent with past reports, in which it was suggested that citrate forms “salt bridges” with certain amino acid groups such as lysine present within BSA.[44]

Table 1 - Characterization data of cit-AuNP and BSA-cit-AuNP

	d_{TEM} (nm)	d_{DLS} (nm)	Electrophoretic mobility ($\mu m \cdot cm \cdot V^{-1} \cdot s^{-1}$)	Zeta potential (mV)
Cit-AuNP	15 ± 6.8 nm	19.7 ± 0.0	-2.05 ± 0.13	-38.4 ± 1.00
BSA-Cit-AuNP	15 ± 6.8 nm	29.4 ± 0.1	-1.95 ± 0.19	-24.6 ± 1.64

A titration experiment was conducted to examine how changes in solution composition affect AuNP surface charging. In this experiment, monovalent (NaCl) and divalent ($CaCl_2$) salt solutions were systematically added to the AuNP suspensions and the electrophoretic mobility was measured. The titration ranges used were deliberately chosen to represent the range of ionic strengths relevant to the column experiments.

An immediate observation can be made based on examination of the titration results (Figure S2). 1) BSA-cit-AuNP consistently had an electrophoretic mobility that was closer to zero than cit-AuNP, despite the addition of salt. Although the trends were not significant, an increase in the ionic strength generally led to a decrease in the magnitude of the electrophoretic mobility values (i.e., a decrease such that the values approach zero). The decrease in surface charge lowers the electro-repulsive interaction between the particles, and suggests that the colloidal suspension becomes increasingly unstable. The decrease in the magnitude of the AuNP electrophoretic mobility values as ionic strength increases was consistent with what has been reported in the literature, as

numerous studies concluded that BSA (or other proteins) effectively mask the electrostatic properties of the particles, essentially making the particle behave more like BSA itself.[52,53] Also, it was worth noting that even though according to the Schultz-Hardy rule Ca^{2+} should have a greater power to destabilize colloidal suspension, the data shown here indicate that given the concentration difference (there was much more NaCl than $CaCl_2$), NaCl was more effective at decreasing the stabilizing repulsive force between the individual AuNP.[54,55]

The soda-lime glass beads used as porous media in the deposition columns were characterized using SEM. As shown in Figure S3, measurement of several of the glass bead images in the SEM micrograph indicate an average size of 260 μm, a value that is consistent with data provided by the manufacturer. Streaming potential measurements of the soda-lime glass beads indicate that they exhibit a highly negative surface charge, but that the magnitude of the charge is a function of the solution pH and the ionic composition of the water it is in contact with. As shown in Figure S4, the surface charge is consistently less negative at an ionic strength of 10 mM set using NaCl relative to a 3 mM ionic strength set using $CaCl_2$.

Evaluation of Gold Nanoparticle Breakthrough. An initial set of experiments was conducted to ensure the robustness of the deposition column system. In the first study, five pore volume (V_{pore}) cit-AuNP pulses of varying concentration were injected into the column and the effluent was monitored using UV-Vis spectroscopy. As shown in Figure 3, the collected breakthrough curves are generally symmetric in shape and are a function of the injected AuNP concentration (C_0) (Figure 3).

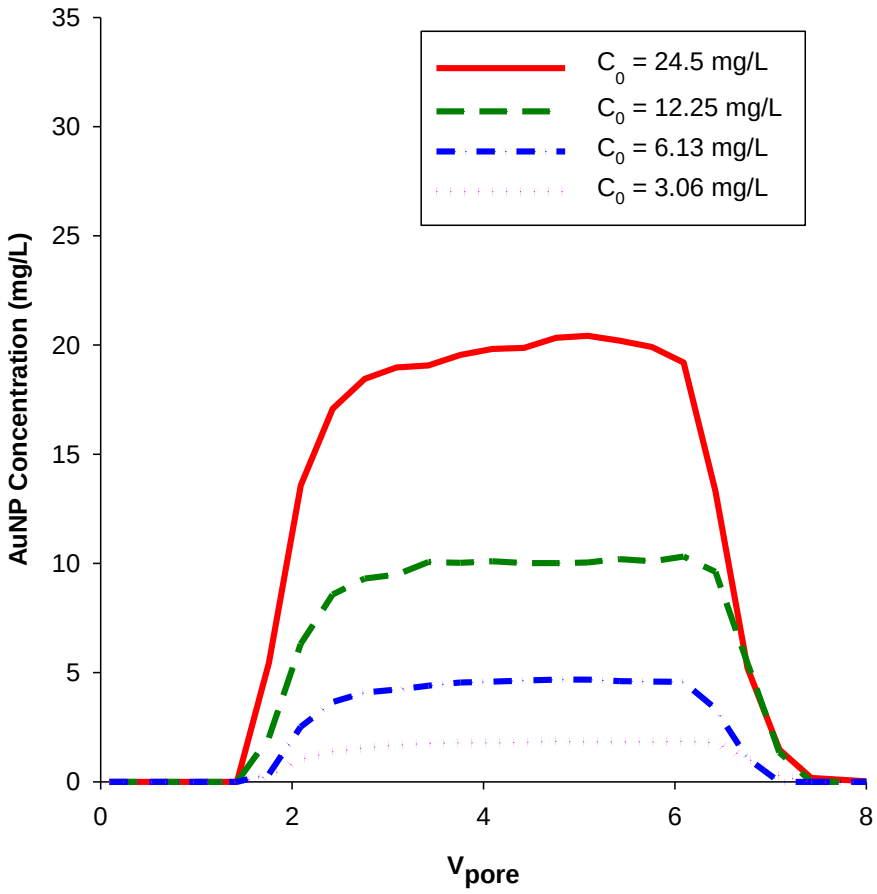

Figure 3 – Cit-AuNP breakthrough curves for varying injection concentration. The diameter of cit-AuNP was 14 nm. Mobile phase contained only 2mM $NaHCO_3$ as a buffer. Injection volume was 5 pore volumes (V_{pore}).

The breakthrough curves depicted in Figure 3 exhibit stable plateaus that scale appropriately with C_0. To ensure the repeatability of the system, eight independent replicates of a 24.5 mg/L cit-AuNP injection were performed. To ensure complete sample independence, the column was repacked between each replicate using clean porous media. All eight replicate breakthrough curves were in agreement with one another and very little variability was observed between runs. Based upon the

consistency of the breakthrough curves in Figure S5 it is apparent that a high degree of reproducibility is possible with the columns.

Nitrate tracer studies performed prior to and after each replicate indicate that no perceptible change in hydraulic residence time was detectable (Figure S6). The lack of such a change indicates that gold nanoparticle retention under these conditions was imperceptible in terms of altering the residence time. Each of the breakthrough curves depicted in Figure 3 and Figure S5 is highly symmetric with an easily defined plateau in the measured effluent AuNP concentration. These breakthrough curves were obtained using a 2 mM $NaHCO_3$ mobile phase in the absence of other salts.

To evaluate the effects of salt addition on cit-AuNP transport and deposition, a series of experiments were conducted in which the number of injected pore volumes was varied between 2 and 30 (Figure 4). In these experiments, the mobile phase contained 30 mM of NaCl in addition to the 2 mM $NaHCO_3$ buffer. NaCl was added to observe how the change in ionic strength would affect the transport of cit-AuNP through the packed column.

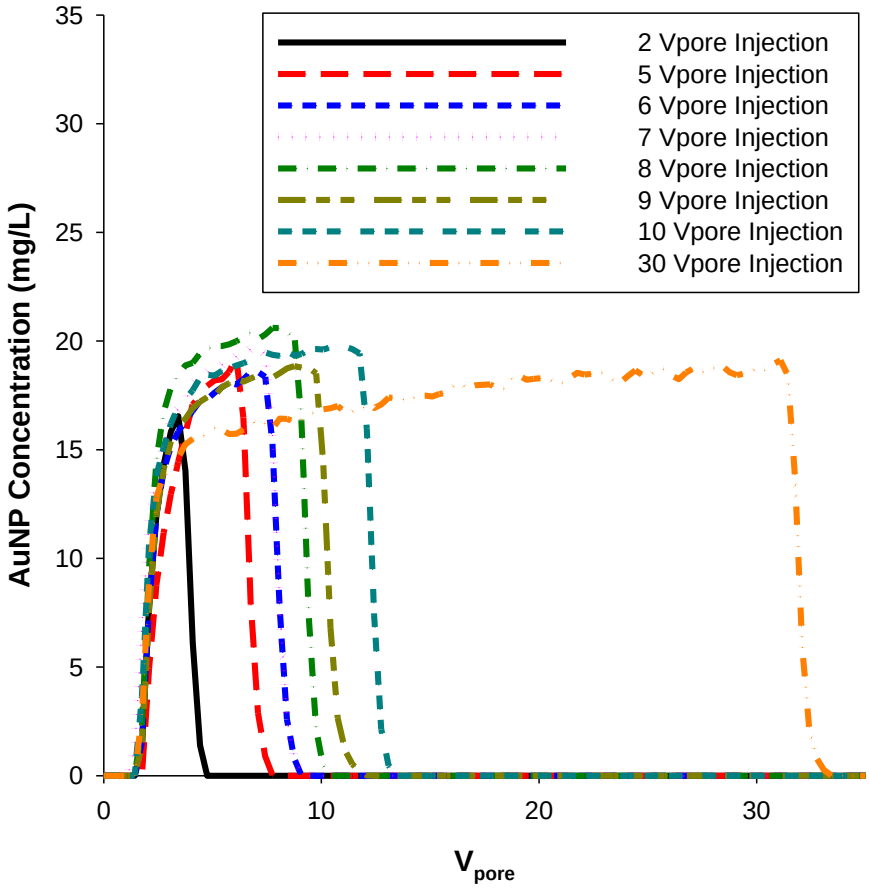

Figure 4 – Cit-AuNP breakthrough curves with varying injection volume. Diameter of citrate AuNP was 14 nm. Mobile phase contained 30 mM NaCl and 2 mM $NaCO_3$ as buffer. C_0 for cit-AuNP was 24.5 mg/L.

Several significant observations can be made regarding Figure 4. Compared to the very symmetric plateaus in Figure 3 when no salts other than the 2 mM $NaHCO_3$ buffer were present, the addition of 30 mM NaCl causes the breakthrough curves to become increasingly less symmetric and the plateau region becomes less well defined (Figure 5).

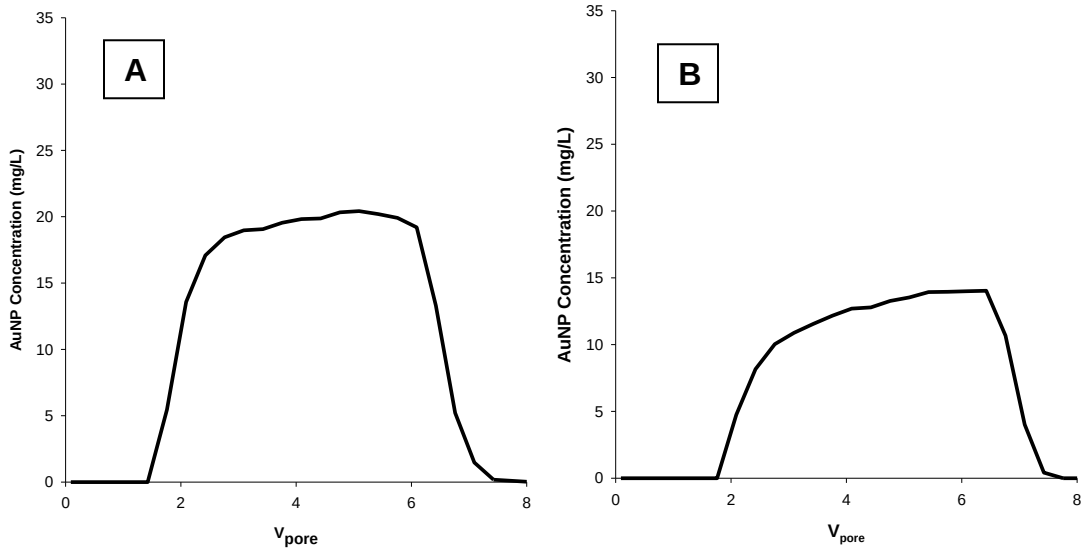

Figure 5 - Cit-AuNP breakthrough curves comparisons. Diameter of citrate AuNP was 14 nm. C_0 for cit-AuNP was 24.5 mg/L. Injection volumn is $5V_{pore}$. Nitrate tracer performed before and after each replicate (data shown elsewhere). A.) Mobile phase only contained 2 mM $NaHCO_3$ as a buffer. B.) Mobile phase contained 2 mM $NaHCO_3$ buffer, and 40 mM NaCl. Note the more asymmetical breakthrough curve in B relative to A.

A possible explanation for the asymmetry of the plateaus after the addition of salt is that there was significant AuNP aggregation and ripening within the pore space of the column, such that equilibrium was never achieved. This hypothesis is supported by the data set shown in Figure 4, particularly the breakthrough curve with 30 V_{pore} injection volumes. Even for a very long injection and sampling time, equilibrium (which would be indicated by a flat plateau) was never reached. Similar slopes in the "plateau region" have been observed in the literature previously. For example, Li *et al.* performed column experiments with *n*C_{60} nanoparticles (produced via the THF method) in a 1.0 mM $CaCl_2$ electrolyte and although they did not discuss it, each of their breakthrough curves exhibited the same asymmetric plateau as the ones observed herein.[35] Solovitch *et al.* performed experiments with TiO_2 nanoparticles and obtained results that were very

similar to those observed here.[42] The breakthrough curve of TiO_2 in the presence of 1 mM NaCl was more symmetric than that of TiO_2 breakthrough obtained in the presence of 40 mM of NaCl.[42]

The asymmetric plateau is indicative of Na^+ ion mediated destabilization of cit-AuNP. Destabilization is indicated by the level of the plateau; in the absence of NaCl the breakthrough curves plateaued at ≈24 mg/L (Figure S5), while in the presence of 30 mM NaCl the breakthrough curves plateaued at ≈18 mg/L (see Figure 5 for comparison).

Effects of $CaCl_2$ and NaCl on AuNP Transport. In order to compare and contrast the transport of cit-AuNP and BSA-cit-AuNP within porous media, column experiments were conducted in the presence of both NaCl and $CaCl_2$ and the results obtained with both types of AuNP were then compared.

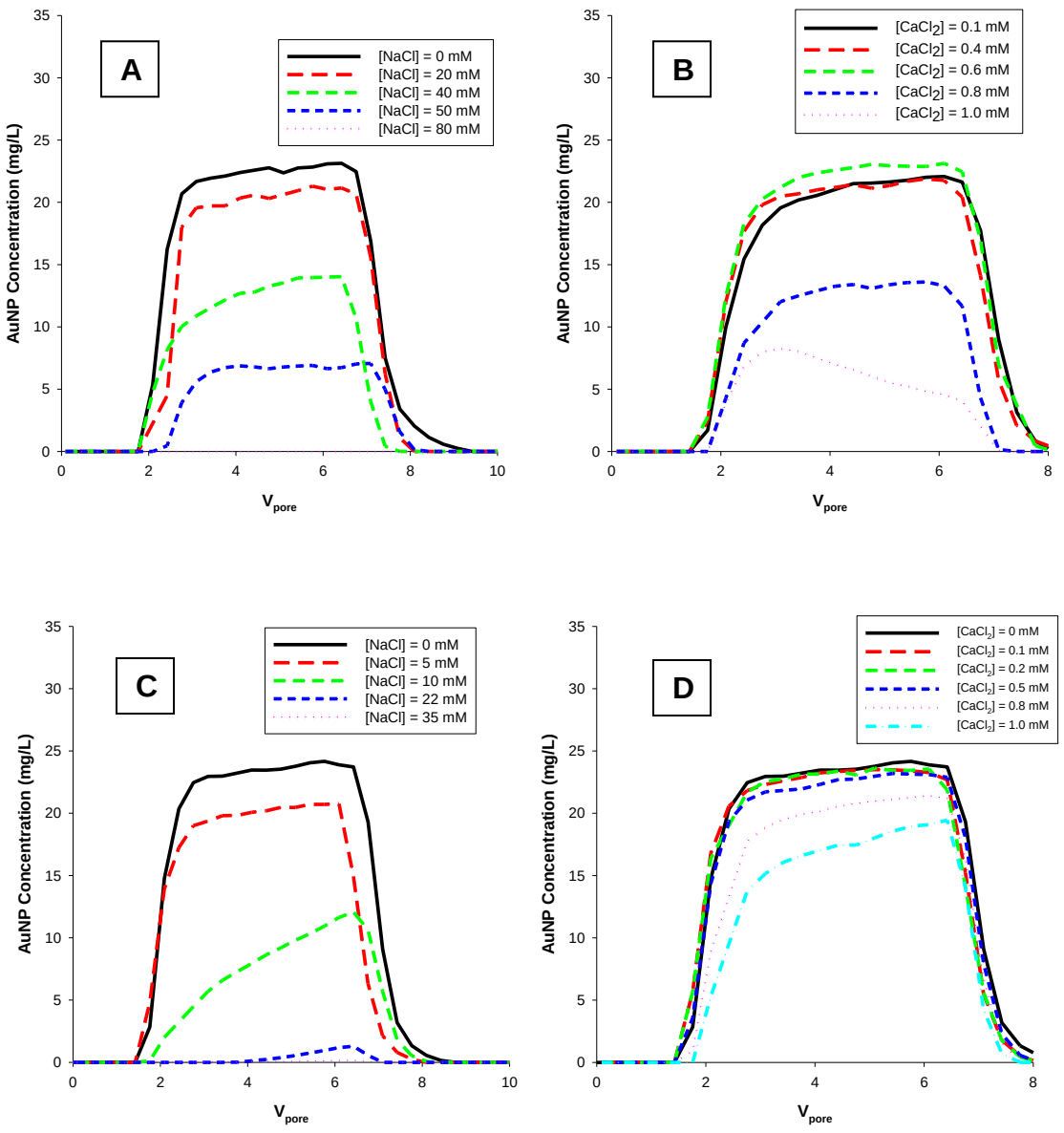

Figure 6 - Citrate-AuNP breakthrough curves with varying [NaCl]. A) cit-AuNP and [NaCl], B) cit-AuNP and [$CaCl_2$], C) BSA-cit-AuNP and [NaCl], and D) BSA-cit-AuNP and [$CaCl_2$].Mobile phase contained a variable amount of NaCl or $CaCl_2$ and 2 mM $NaCO_3$ as buffer. Diameter of citrate AuNP was 14 nm. C_0 for cit-AuNP was 24.5 mg/L; C_0 for BSA-cit-AuNP is 25.4 mg/L. Additional data set was obtained at different [NaCl] level, but only a selected few is presented here for readability.

Cit-AuNP Column Experiments. Experiments with variable NaCl showed that as the mobile phase NaCl concentration increased that larger amounts of cit-AuNP were retained in the column. This result is in agreement with the hypothesis that an

increase in ionic strength destabilizes AuNP suspensions. To further probe this phenomenon, divalent Ca^{2+} was used in place of Na^{+} as the incremental salt addition. According to the Schultz-Hardy rule, a higher valence ion should have a greater destabilizing effect on the colloidal suspension, thus leading to more effective aggregation of AuNP within the pore space of the column.[54,55] There was also evidence that a higher valence cation such as Ca^{2+} would lead to more efficient deposition of AuNP onto the porous media within the column.[56] Ions of higher valence are known to shield the stabilizing interaction of the electron double layer of the surfaces of the AuNP and glass beads, decreasing their electrostatic potentials and repulsion energies.[56]

The assumption that divalent ions destabilize the cit-AuNP system better than monovalent ions was confirmed by the experimental results (Figure 6, A and B). Much lower concentrations of $CaCl_2$ were required to achieve similar amounts of cit-AuNP retention in the column. This result is consistent with previously reported results. In a study conducted by Espinasse *et al*. examining nC_{60} transport 10 mM of $CaCl_2$ and 60 mM of NaCl produced similar breakthrough curves.[33] A notable observation from the results in Figure 6A and Figure 6B is the slope in the plateau region. This slope corroborates with the observed slope in the previous experiments examining cit-AuNP transport as a function of the number of pore volumes injected in the presence of 30 mM NaCl (Figure 4). The slope becomes increasingly severe with an increase in ionic strength. This trend is consistent with what others have observed in column transport and deposition studies.[34,35,42] This result make sense because as the mobile phase ionic strength increases, the cit-AuNP suspension becomes less and less stable, thus

increasing deposition and aggregation. The change in deposition and aggregation rates leads to breakthrough curve plateaus that are highly unstable.

Evaluation of the affinity between collector media and AuNP. To investigate the attributes between the glass beads and the cit-AuNP, a series of batch experiments were performed. The batch reactors contained a pH buffer (2 mM $NaHCO_3$, the same type and concentration used in the column experiments) and cit-AuNP (at the C_0 concentration of the column experiment, that is, 24.5 mg/L). Half of the reactors contained 10 g of glass beads, while the other half did not. The reactors without glass beads served as experimental controls. The reactors were adjusted to a specific pH and [NaCl]. The results of the array of batch reactor experiments are summarized in Figure S7.

The results from the batch experiments overwhelmingly suggest that the glass beads initiated or magnified physiochemical changes to the cit-AuNP that caused the loss of nanoparticles from suspension due to either aggregation and/or deposition. This could be clearly observed when comparing results of the batch reactors at the same pH and [NaCl] (Figure S7). Cit-AuNP levels inside reactors that contained glass beads clearly experienced a faster drop in detectable concentration relative to those that were in reactors that did not contain any glass beads. Another important observation can be made while focusing on the first row of the bar graphs. The row of results was from reactors that contained no NaCl at all (but only a small amount of $NaHCO_3$). Under these conditions a portion of the cit-AuNP in reactors that contained glass beads became undetectable by the UV-Vis as time progressed. Examination of the location of the plasmon resonance band in the UV-Vis spectrum for samples from the reactors that

contained glass beads, the peak wavelength experienced a significant red shift as time progressed (Figure S8).

The observed red shift provides strong evidence of a heteroaggregation process.[57,58] The significance of this result is that NaCl was not the sole agent facilitating AuNP aggregation because it was not present in these reactors. It is highly likely that a surface interaction between the citrate-AuNP and the glass beads (predominantly silica) was inducing AuNP heteroaggregation to the surface of the glass beads. This may be evidence pointing to the occurrence of significant ripening of the glass bead surface in the column. Ripening of the porous media occurs when nanoparticles in the column pore space deposit on to the surface of a porous media grain that has already been covered by nanoparticles.

BSA-cit-AuNP Column Experiments. In addition to conducting transport experiments using cit-AuNP, a series of column experiments were also conducted using BSA-cit-AuNP. The collected breakthrough curves in the presence of NaCl and $CaCl_2$ are shown in Figure 6C and Figure 6D. BSA stabilized AuNP has previously been found to be more resistant to ionic destabilization than cit-AuNP (Hull, M. unpublished data). The BSA layer provides an electrosteric repulsive interaction between AuNP, leading to a more stabilized suspension. As shown in the DLS data (Table 1), the hydrodynamic diameter of cit-AuNP increases after addition of BSA. This change is expected to effectively increase steric hindrance between individual nanoparticles of BSA-cit-AuNP, as well as between BSA-cit-AuNP and the glass beads, which in turn was expected to result in less efficient deposition and aggregation.

Based upon its resistance to salt induced aggregation in suspension, BSA-cit-AuNP was expected to be less susceptible to deposition in the presence of high concentrations of salt. As shown in Figure 6C, this expectation was not observed for NaCl; in contrast however, the expectation was met for $CaCl_2$ (Figure 6D). The plateaus of each of the breakthrough curves in Figure 6D only decreased slightly as [$CaCl_2$] increased. Conversely, at similar concentrations of $CaCl_2$, a very high percentage of cit-AuNP was retained in the column (Figure 6B). The experimental results with BSA-cit-AuNP in the presence of NaCl were unexpected. Because batch data from previous experiments (Hull, M., unpublished results) had clearly indicated that BSA-cit-AuNP exhibits greater colloidal stability in the presence of high concentrations of salt than cit-AuNP, it was expected that there would be little to no retention of BSA-cit-AuNP in the column. In other words, it was expected that the plateau would experience little decrease in height as [NaCl] increased, as was observed in the $CaCl_2$ breakthrough curves. However, this hypothesis was not what was supported. Instead, a smaller amount of [NaCl] was needed to achieve the same level of AuNP retention when compared to the same experiment conducted with cit-AuNP.

The breakthrough curves in Figure 6C seemed to suggest that BSA-cit-AuNP has a very high affinity for the glass beads in the column in the presence of NaCl; however, Figure 6D suggests that this enhanced association was not observed for $CaCl_2$. Although the $CaCl_2$ levels used in the experiments depicted in Figure 6D are considerably lower than those of NaCl, the $CaCl_2$ levels covered the same range as those used to comparatively deposit cit-AuNP (Figure 6B).

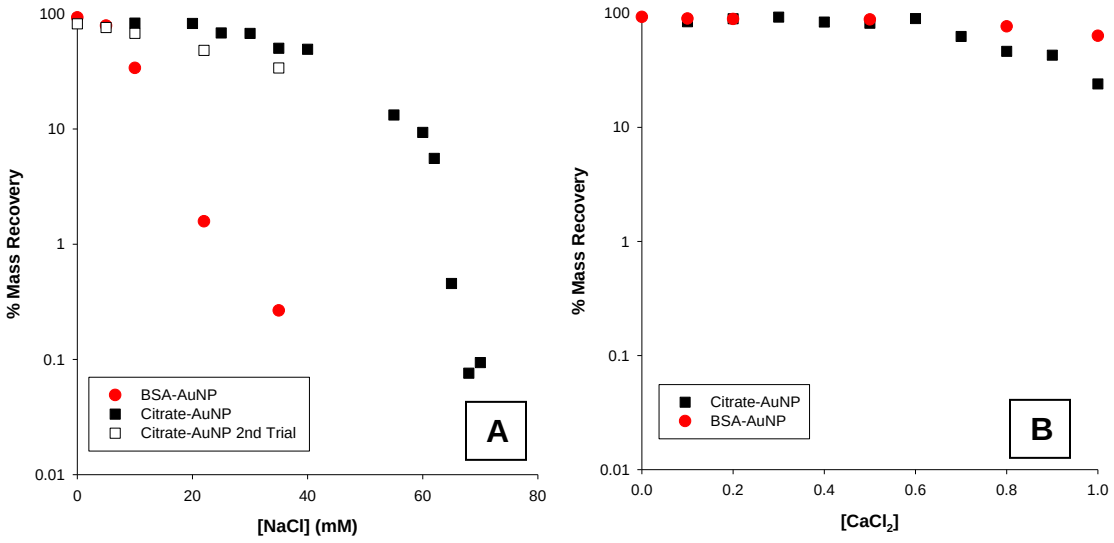

Figure 7 - Mass retention of AuNP with increasing A) [NaCl] and B) [$CaCl_2$]. Results obtained by integrating the area beneath the breakthrough curves from the respective experiments.

The discrepancy between the studies depicted in Figure 6 is most easily visualized in Figure 7A. In this figure, the experimental results from the breakthrough curves of the two varieties of AuNP and NaCl addition are summarized in a scatter plot. It is notable that the trend observed here was the opposite of what was predicted. For example, at 22 mM of NaCl, ≈70% of cit-AuNP were recovered from the column outflow, while only ≈3% of the BSA-AuNP were recovered. The trend observed for $CaCl_2$ addition instead was in agreement of the initial hypothesis (Figure 7B) that BSA-cit-AuNP will be resistant to salt-induced destabilization relative to cit-AuNP. As expected, BSA-cit-AuNP was more stabilized and resistant to $CaCl_2$'s destabilizing effects. The effect of NaCl on BSA-cit-AuNP during the column experiment deviated from the initial hypothesis. This deviation to the hypothesis was particularly evident when looking at the 1 mM data point in Figure 7A, where ≈70% of BSA-cit-AuNP was recovered from the

column outflow, but only ≈20% of cit-AuNP was recovered. The result in Figure 6 and Figure 7 can be explained when the zeta potantial values of the BSA-cit-AuNP and glass beads are taken into account (Table 2).

Table 2 - Summary of zeta potential data during column experiments; ranging through all salt concentrations

Experiment	Glass Beads Zeta Potential Range	AuNP Zeta Potential Range
Cit-AuNP + NaCl	-80 to -32 mV	-42 to -29 mV
Cit-AuNP +$CaCl_2$	-80 to -55 mV	-42 to -35 mV
BSA-Cit-AuNP + NaCl	-80 to -32 mV	-27 to -18 mV
BSA-Cit-AuNP + $CaCl_2$	-80 to -55 mV	-35 to -27 mV

Looking at Table 2, it can be seen that for the column experiments that involved BSA-cit-AuNP and NaCl, both the glass beads and the nanoparticles had zeta potential values that were nearly neutral. Especially for BSA-cit-AuNP; in the upper range of [NaCl] its zeta potential was as high as ≈ 18 mV. Generally, BSA-cit-AuNP were more colloidally stable than cit-AuNP. Results from batch experiments (Hull, M., unpublished data) and the column experiment between BSA-cit-AuNP and $CaCl_2$ confirmed this. It was very likely that the stabilizing effect BSA had on AuNP was not related to zeta potential, but as mentioned above, a mix of electrostatic (from zwitterionic charged points on the protein molecule) and steric repulsion. However, in the column experiments involving both BSA-cit-AuNP and NaCl, the combined effect of a very neutral zeta potential (the nanoparticle was still negatively charged, but relatively weakly when compared to the other cases) of the nanoparticles and the glass beads likely overcame whatever electrosteric stabilizing effect BSA had, resulting in rapid

aggregation or deposition within the column. This fast interaction rate was not observed in the cit-AuNP column experiment with NaCl, because the negative zeta potential of cit-AuNP was still quite large under the experimental environment.

Quantitative evaluation of nanoparticle transport. To understand the mechanism governing the retention of AuNP in the column, the single-cell filtration attachment efficiency can be calculated:[27]

$$\alpha = -\ln\left(\frac{C}{C_0}\right)\frac{(4a_c)}{3(1-\epsilon)\eta_0 L} \quad (6)$$

Where C is the plateau concentration of the corresponding AuNP breakthrough curve, C_0 is the initial inflow concentration, a_c is the radius of the glass beads, ϵ is the porosity of the packed column, L is the length of the packed column and η_0 is the collector efficiency as calculated using the correlation developed by Tufenkji and Elimenech.[28]

Each calculated α denotes a ratio between AuNP that successfully made collision with a glass bead, and those that remained attached after.[29,59] Therefore, $\alpha = 1$ means that all collisions between AuNP and the glass bead surface led to attachment. In the equation, η_0 (collection efficiency) was of particular importance because it encompasses a large amount of information and parameters pertinent to describing the transport environment within the column. These parameters included Brownian diffusion, gravitational sedimentation, and interception (advection).[28] Tufenkji and Elimelech developed a vigorous correlation to calculate this parameter:

$$\eta_0 = \eta_D + \eta_I + \eta_G \quad (7)$$

where η_D is the portion of the correlation accounting for diffusion, η_I for advection and η_G for gravitational effects. Equation (7) expends to:

$$\eta_0 = 2.4A_S^{1/3}N_R^{-0.081}N_{Pe}^{-0.715}N_{vdW}^{-0.052} + 0.55A_S N_R^{1.675}N_A^{0.125} + 0.22N_R^{-0.24}N_G^{1.11}N_{vdW}^{0.053} \quad (8)$$

where A_S is a porosity parameter; N_R is the aspect ratio between the porous media and the AuNP; N_{Pe} is the Péclet number; N_G is a dimensionless gravity parameter, N_A is a dimensionless parameter accounting for attraction between AuNP and the porous media, and N_{vdW} is a dimensionless parameter accounting for van der Waals interaction. These parameters are in turn defined as:

$$A_S = \frac{2(1-\gamma^5)}{2-3\gamma+3\gamma^5-2\gamma^6} \qquad \gamma = (1-f)^{1/3} \quad (9)$$

$$N_R = \frac{d_p}{d_c} \quad (10)$$

$$N_{Pe} = \frac{Ud_c}{D_\infty} \quad (11)$$

$$N_G = \frac{2}{g}\frac{a_p^2(\rho_p - \rho_f)g}{\mu U} \quad (12)$$

$$N_A = \frac{A}{12\pi\mu a_p^2 U} \quad (13)$$

$$N_{vdW} = \frac{A}{kT} \quad (14)$$

where f is porosity, d_p is the AuNP diameter, d_c is the glass bead diameter, U is the fluid approach velocity, D_∞ is the bulk diffusion coefficient as determined by the Stokes-Einstein equation, A is the Hamaker constant, k is the Boltzmann constant, T is the fluid absolute temperature, a_p is the radius of AuNP, ρ_p is the density of AuNP, ρ_f is the density of the fluid, μ is the absolute fluid viscosity, and g is the gravitational acceleration. Using the parameters listed in Table 3, the individual dimensionless terms in Equation (8) were calculated for the present system (Table 3 and Table 4)

Table 3 – Input parameters for the calculation of the collector efficiency (η_0)

Boltzmann constant (k_B)	1.38×10^{-23} J/K
Gravitational acceleration (g)	9.81 m/s^2
Particle diameter (d_p)	14 nm
Particle radius (a_p)	7 nm
Collector diameter (d_c)	250 μm
Approach velocity of fluid (U)	2.36×10^{-4} m/s
Hamaker constant (A)	3.2×10^{-20} J (obtained from literature[60])
Temperature (T)	298 K
Particle density (ρ_p)	19.3 g/cm^3
Fluid density (ρ_f)	0.9998 g/cm^3
Absolute (dynamic) viscosity of fluid (μ)	0.0009 N·s/m^2
Porosity (f)	0.34
Gamma (γ)	0.871
Porosity-dependent parameter (A_s)	56.39

Table 4 - Dimensionless parameters for the calculation of collector efficiency (η_0)

N_R	5.60×10^{-5}
N_{Pe}	1.70×10^{3}
N_{vdW}	7.78
N_A	1.67×10^{18}
N_G	9.22×10^{-9}

Combining Table 4 and Equation (8), $\boldsymbol{\eta_0 = 0.111}$. It is important to note that the terms

related to Brownian diffusion in Equation (8) essentially dominates η_0, such that for this study:

$$\eta_0 \cong 2.4A_S^{1/3}N_R^{-0.081}N_{Pe}^{-0.715}N_{vdW}^{-0.052} \quad (15)$$

The elimination of the gravitational and diffusion terms was consistent with what was expected (i.e., the mass of the individual AuNP was too small for them to be meaningfully sedimented by gravity and the average size of the AuNP are at a point where Brownian motion generally dominates (< 0.1 μm)).[3] Similar conclusions and observations were obtained by others performing similar calculations and experiments.[29]

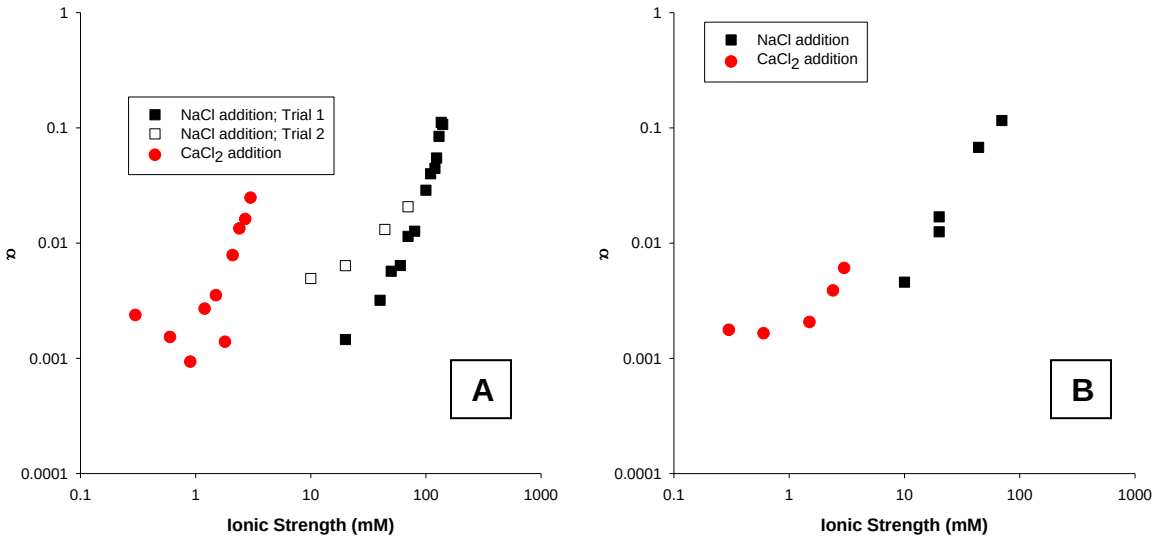

Figure 8 - Attachment efficiencies (α) of cit-auNP with increasing ionic strength. A) Data with cit-AuNP; B) data with BSA-cit-AuNP

α values calculated using Equation (6) were plotted as a function of the solution ionic strength to visualize the effects of salt addition on the attachment efficiencies. In Figure 8A, it is obvious that even though the ionic strengths for the $CaCl_2$ experiments were much lower than those used in the NaCl experiments they were still sufficient to drive

the values of α up to about the same level achieved with much higher NaCl concentrations.

Looking at the calculated α from the BSA-cit-AuNP column experiments, the results agree with the observations from column experiments (Figure 8B). When compared to the previous plot (Figure 8A), the α values for the $CaCl_2$ experiments did not rise as sharply as in the same experiment conducted with citrate-AuNP. This slower rise of the α values for the BSA-cit-AuNP and $CaCl_2$ makes sense because there was not as much BSA-cit-AuNP retention than cit-AuNP under the same $CaCl_2$ conditions. The rising slope of the NaCl data points (for BSA-cit-AuNP, black square plot in Figure 8B) was much steeper compared to the rising slope of the $CaCl_2$ data points (for BSA-cit-AuNP, red circle plot in Figure 8B). This was reflective of the unexpected high BSA-cit-AuNP retention with NaCl addition.

A common anomaly observed in both sets of α values calculations (from both cit-AuNP and BSA-cit-AuNP) is that the α values are strikingly low given the amount of AuNP retention that was observed. For example, in Figure 8B a data point of ionic strength ≈100 mM gave an α value of ≈10%. This result would suggest that 10% of the BSA-cit-AuNP that collided with the glass beads in the column stayed attached, and consequently were retained in the column. However, upon comparing this α value to the corresponding actual mass recovery (see Figure 6C, specifically the data point at 50 mM NaCl for BSA-cit-AuNP) ≈90% of the BSA-cit-AuNP was retained in the column. The same discrepancy between α values and the actual retention of AuNP was observed throughout all of the collected data. This trend of extremely small α values

was particularly intriguing especially when compared to results obtained by others who had done similar experiments. Generally all column deposition studies done on nanomaterials resulted in α values that asymptotically approach 1.[33,36–39,41,56,61] This result observed by others is logical because their collected breakthrough curve often exhibit low C/C_0 values at high ionic strength. As C/C_0 approached 0, α should approach 1. Recall that if α = 1, it means that all AuNP that made contact with a collector (i.e., a glass bead) stayed attached to the collector. If this was the case, it would imply that breakthrough curves obtained at a high ionic strength, which exhibited very low mass recovery and C/C_0, were heavily depositing AuNP onto the surface of the glass beads along the column. Yet, since we *do* observe low mass recovery and C/C_0 , but *not* a corresponding high α value, this heavy deposition along the column was clearly not what was happening.

Recently, Solovitch *et al.* encountered similarly low α values when conducting column experiments using TiO_2 nanoparticle.[42] From their results, the calculated α values ranged from 0.04 to 0.09. Solovitch attributed this to the fact that Equation (6) and (7) did not account for two important processes within the column. One was that of significant NP aggregation within the pore space. As shown with the previous batch experiment, the presence of the glass beads increases the rate of cit-AuNP aggregation. It was very likely that a large amount of AuNP retained in the column had aggregated in solution and was retained either via physical straining or physiochemical interactions with the porous media. Another process not accounted for in the calculation of η_0 and α was the process of ripening. Ripening refers to the deposition of AuNP onto AuNP that had already deposited onto a porous media grain. Both of these theories were

supported by the batch experiment results (Figure S7 and Figure S8). If there was an interfacial interaction between AuNP and the porous media that caused the nanoparticles to aggregate significantly within the column pore space, which can than lead to AuNP ripening of the glass bead surfaces, this could explain the discrepancy between mass recovery of the column experiments, and the calculated attachment efficiencies.

In this case then, the very low α values were not erroneous, but rather only describe a portion of what was occurring within the column. The very low α values (< 10%) suggest the attachment processes accounted for within the calculation of η_0 have very little contribution to AuNP retention within the column. In the case of the experiments performed here, η_0 was dominated by Brownian diffusion. The mass retention of AuNP not accounted for is then likely due to very favorable aggregation of the nanoparticles within the pore space of the column, leading to subsequent (or perhaps, concurrent) ripening of the surface of the porous media.

Investigation of possible retention of AuNP in column pore space through significant aggregation and ripening via DLVO theory. At this point the hypothesis that was made in the previous section – significant aggregation and ripening of AuNP not accounted for in α values – has only been supported by circumstantial evidence and postulations. To investigate the merit of this hypothesis, DLVO theory was utilized to explore in detail what the actual interfacial interactions are between the various solid phases in the column. DLVO theory was developed independently by Dejaguin with Landau, and Verway with Overbeek.[30,31] DLVO theory states that the interaction

between colloidal surfaces is comprised of the Lifshitz-van der Waals (LW) interaction and the electrostatic (EL) interaction.[3] This in practice can be expressed formally as:

$$U_{123}^{DLVO} = U_{123}^{LW} + U_{123}^{EL} \quad (16)$$

where U_{123}^{DLVO} is the total interaction energy between surfaces 1 and 3 suspended in liquid media 2, U_{123}^{LW} and U_{123}^{EL} are the energy contributions from the Lifshitz-van der Waals interaction and the electrostatic interaction, respectively.

The Lifshitz-van der Waals interaction accounts for electrodynamic interactions between surfaces in aqueous media, these include the dispersion due to dipole interactions between surfaces, the change in orientation due to dipole interactions, and the dispersion of surfaces in the media via dipole interactions.[62] When considering the interaction between a single AuNP and a grain of porous media in the column, it is helpful to approximate such interactions to be between a perfect sphere and an infinitely long plate. This approximation is appropriate because relative to the size of a AuNP, the glass bead grain is much larger, effectively functioning like a flat plane. Derjaguin provided an approximation for U_{123}^{LW} as follows:

$$U_{123}^{LW} = -\left(\frac{A\alpha_p}{6h}\right)\left(1 + \frac{14h}{\lambda}\right)^{-1} \quad (17)$$

where A is the Hamaker constant between the surfaces that are interacting (in this case AuNP and glass); α_P is the radius of the AuNP, h is the distance between the interacting

surfaces, and λ is the characteristic wavelength of the dielectric, which is typically estimated to be 100 nm.[3]

To examine whether there was significant aggregation between particles, the above approximation cannot be used. The interaction between two spherical AuNP of similar size is very different from the interaction between a spherical particle and a flat plane.[63] As such, a different approximation must be used:

$$U_{121}^{LW} = -\left(\frac{A}{6}\right)\left\{\left[\frac{2a_p^2}{h\left(4a_p + h\right)}\right] + \left[\frac{2a_p^2}{2\left(a_p + h\right)^2}\right] + \ln\left[\frac{h\left(4a_p + h\right)}{\left(2a_p + h\right)^2}\right]\right\} \quad (18)$$

In order for a colloidal suspension to remain stable according to DLVO theory, there must be an opposing interaction counteracting the Lifshitz-van der Waals attraction. In DLVO theory, the total interaction energy between two surfaces suspended in a medium must also account for the electrostatic interactions between those two surfaces. Modeling electrostatic interactions is very complex, and usually simplifications must be made for the approximation. Common approximations usually either hold the electric potential of the surfaces to be constant, or the electric charge of the surfaces to be constant.[64] The model used here was developed by Hogg *et al.*, which assumes constant surface potential.[65] The expression is as follows:

$$U_{123}^{EL} = \pi\varepsilon_r\varepsilon_0 a_p\left[2\zeta_1\zeta_3\ln\left(\frac{1 + e^{-\kappa h}}{1 - e^{-\kappa h}}\right) + (\zeta_1^2 + \zeta_3^2)\ln(1 - e^{-2\kappa h})\right] \quad (19)$$

Where U_{123}^{EL} is the electrostatic interaction energy between surface 1 and surface 3 dispersed in medium 2; $\varepsilon_r\varepsilon_0$ is the dielectric permittivity of the suspending fluid (in this case, the value of water at 298 K was used; $6.95 \times 10^{-10} F \cdot m$); α_p is the radius of the AuNP, ζ_1 and ζ_3 are the surface potential of the interacting surfaces (zeta potentials obtained from particle analyzer were used here); h is the distance between interacting surfaces; and κ is the inverse Debye length, which is defined as:

$$\kappa = \sqrt{\frac{e^2 \sum n_i z_i^2}{\varepsilon_r \varepsilon_0 kT}} \tag{20}$$

Where e is the electron charge; n_i and z_i are the number concentration and valence of ion i; k is the Boltzmann constant,$\varepsilon_r\varepsilon_0$ is the dielectric permittivity of the suspending fluid, and T is the absolute temperature of the environment. For the electrostatic interaction between two AuNP (assuming that both are perfect spheres), some simplification can be made:

$$U_{121}^{EL} = 2\pi\varepsilon_r\varepsilon_0 a_p \zeta_1^2 \ln(1 + e^{-\kappa h}) \tag{21}$$

Combining both the energy contribution from Lifshitz-van der Waals interaction (U^{LW}) and the electrostatic interaction (U^{EL}), the net total colloidal surface interaction energy can be calculated (U, see equation (16)). Generally speaking, when U is positive the net interaction is repulsive, and when U is negative, the net interaction is attractive.[3] Colloidal surface interactions due to AuNP-glass bead deposition energy (U_{123}, using equation (17) and (19)) or AuNP-AuNP aggregation energy (U_{121}, using equation (18)

and (21)) was assumed to be the two main interactions occurring. By plotting these interaction energy levels with respect to distance between the two interacting surfaces, the resultant plot will reveal information regarding what is occurring within the packed columns during an experiment, above and beyond those that were described by attachment efficiencies (α) and collector efficiencies (η_0).

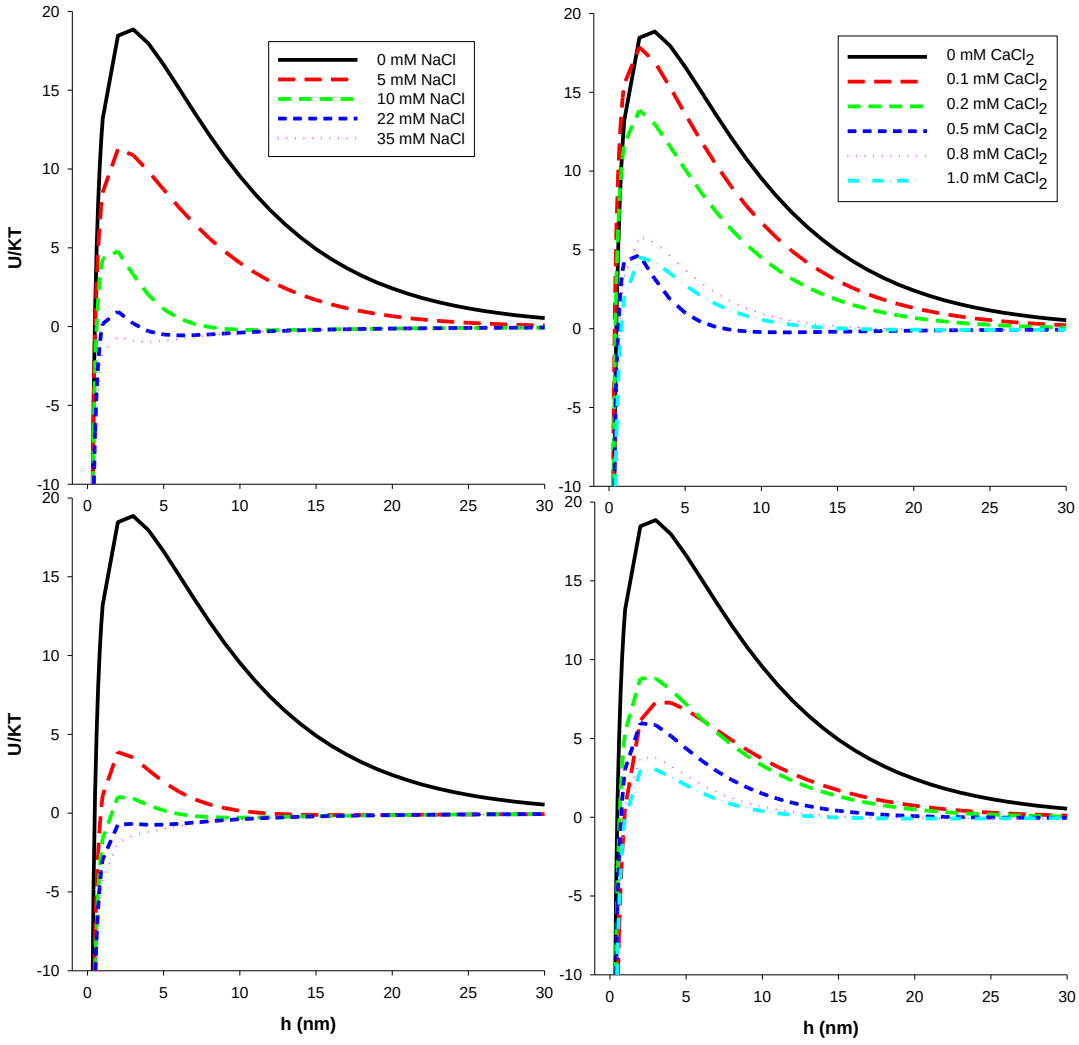

Figure 9 – DLVO plot describing *deposition interaction* between AuNP and glass beads using equation (17) and (19). Clockwise from upper-left: cit-AuNP with increasing [NaCl]; cit-AuNP with increasing [$CaCl_2$]; BSA-cit-AuNP with increasing [$CaCl_2$]; and BSA-cit-AuNP with increasing [NaCl]

Several observations from the DLVO plots for deposition interaction (Figure 9) are notable. First of all, these DLVO curves agreed with the hypothesis and experimental observation that a much lower concentration of Ca^{2+} (a divalent cation) was needed to achieve the similar deposition behavior observed with a higher concentration of Na^{+} (monovalent cation). The scale of all the plots in the interaction curve (Figure 9) are the same, and the actual curves themselves were very similar in the range of U/KT values, yet the actual concentration range of the salt between NaCl and $CaCl_2$ was very different. Secondly, the primary peak (the maximum of each energy plot) provided very important information regarding on AuNP deposition onto glass beads. Recall that if U/KT is positive, the overall interaction between the two surfaces will be repulsive. The primary peak then, represents the energy barrier the surfaces need to overcome before irreversible attachment (in this case, deposition) will occur. Upon comparing the primary peak between the plots from cit-AuNP and BSA-cit-AuNP, the primary peaks on the BSA-cit-AuNP curves were significantly lower than the cit-AuNP counterpart. This difference in the energy barrier height is noticeably higher at lower salt concentration. It seems to suggest that at low (but present) cation concentrations, the BSA-cit coating on the AuNP was not effective in shielding deposition interaction between the glass bead surface and the AuNP. At higher concentrations of cation, the deposition interaction energy between the cit-AuNP and BSA-cit-AuNP was much more similar. This narrowing of the primary peak energy gap between cit-AuNP and BSA-cit-AuNP agrees with the experimental observation. Recall that in the breakthrough curves of cit-AuNP and BSA-cit-AuNP with varying NaCl concentration (Figure 6A and C), the breakthrough curve plateaus of the BSA-cit-AuNP

decreases much more rapidly than those of the cit-AuNP curves; however at very high NaCl concentration the two curves were similar in level. Finally, this set of deposition DLVO curves provided some possible explanation to why BSA-cit-AuNP were much less resistant to NaCl than to $CaCl_2$. Recall from the breakthrough curves of BSA-cit-AuNP with increasing $CaCl_2$ concentration (Figure 6D), the plateaus of the curves decrease less rapidly than those from the cit-AuNP curves (Figure 6B). However, the exact opposite was observed in the NaCl experiments; with increasing NaCl concentration, BSA-cit-AuNP breakthrough curve plateaus decreases rapidly than those from cit-AuNP (Figure 6A and C). This result was in disagreement with the hypothesis, which stated that BSA-cit-AuNP should be more resistant to destabilization via increases in ionic strength. Attempts to explain this discrepancy in ionic strength resistance with colloidal filtration theory (α and η_0) did not yield any satisfactory conclusion. However, while the DLVO plots (Figure 9) seems to suggest that while BSA-cit-AuNP as a whole exhibit a lower energy barrier for irreversible deposition than cit-AuNP, since all primary peaks from BSA-cit-AuNP is lower to their corresponding ones from cit-AuNP, the gap in the difference between corresponding primary peak height is narrower for the case with $CaCl_2$. In some cases, the primary peak height from the BSA-cit-AuNP plots (with $CaCl_2$) is higher or at the same level as the ones from cit-AuNP, usually at higher Ca^{2+} level. This implies that at high Ca^{2+} level, BSA-cit-AuNP should exhibit similar if not better resistance to destabilization effect due to salt concentration.

All of the above analyses were only considering the uninterfered deposition interaction between one single AuNP and the glass bead surface (modeled as an infinite plane). However, the aggregation effect between two (or realistically, more)

AuNP must also be considered. In fact, this omission is possibly the main reason colloidal filtration theory did not accurately describe the experimental results.

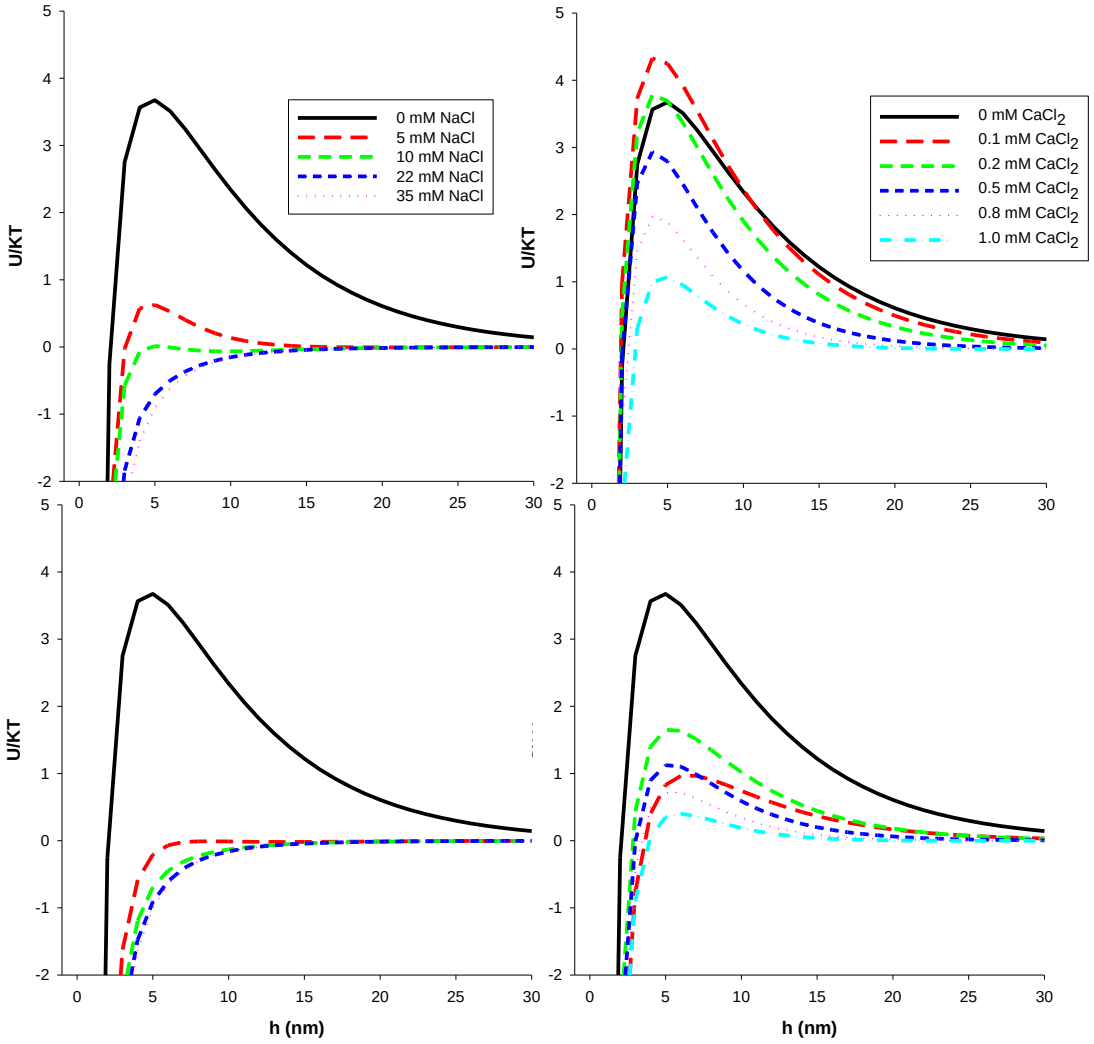

Figure 10 - DLVO plot describing *aggregation interaction* between two AuNP using equation (17) and (19). Clockwise from upper-left: cit-AuNP with increasing [NaCl]; cit-AuNP with increasing [$CaCl_2$]; BSA-cit-AuNP with increasing [$CaCl_2$]; and BSA-cit-AuNP with increasing [NaCl]

When considering the DLVO plots for aggregation effects (using equation (18) and (21)), the results are telling (Figure 10). The first immediate observation was that all of the energy level for aggregation were much lower than those for deposition (Figure 9). The

energy barrier for deposition can be as high as 20 (dimensionless, U/KT), while for aggregation the maximum height of the interaction energy level for all considered cases was at ≈ 4.5. Furthermore, the locations of the primary peaks were different as well. For deposition, the maximum energy barrier is located ≈ 2 nm; while for aggregation, the barrier is located at ≈ 5 nm. The means that the interacting surfaces have a higher probability to aggregate than to deposit, since they do not have to be as close to each other for irreversible attachment to occur.

Another important observation from the DLVO plots of aggregation interaction (Figure 10) was that even a small amount of NaCl completely collapsed the energy barrier for BSA-cit-AuNP. This effectively means that from a DLVO standpoint, even at the lowest experimental concentration of NaCl (in this case 5 mM), there was no repulsive interaction preventing the nanoparticles to aggregate. On the other hand, with $CaCl_2$ BSA-cit-AuNP still exhibited a decrease in energy barrier level, but the barrier was at least still present. This result may explain the experimental observation that BSA-cit-AuNP were not resistant to NaCl destabilization. Since at the NaCl level the experiments were run under, there was no DLVO repulsion to prevent aggregation, the BSA-cit-AuNP were probably heavily aggregating within the pore space of the packed column. This rapid aggregation may be why there was heavy retention of the nanoparticles within the column. The hypothesis (BSA-cit-AuNP more stable; Schulz-Hardy rule applies) and colloidal filtration theory failed to predict this because pore space aggregation of particles were not considered or deemed negligible. An important fact to remember is that both DLVO plot arrays (Figure 9 and Figure 10) cannot be used to quantitatively describe what was happening in the experiment, since the DLVO

calculation only considers a one-to-one interaction (i.e., one particle versus one infinite surface, or one particle versus another particle). In reality, much more complex interactions were occurring. Simultaneous deposition of multiple particles onto the same surface, for example, was very likely to be occurring. The energetics of such interaction can be unpredictable. Another major caveat of the DLVO calculation was that it assumes the sizes of the AuNP stay constant. This assumption cannot be true if aggregation is occurring, which as shown above was most definitely. If aggregates of nanoparticles are considered to be larger “particles”, their deposition (and possibly further aggregation) interaction and energetics will deviate from the DLVO plots. While DLVO calculations and analyses were able to fill in some holes that colloidal filtration theory had left, it was not a perfect description of the complete physio-chemical processes of AuNP transport within an aqueous porous environment.

Chapter 4 – Conclusion

The original hypothesis and goal for this project was to evaluate how functionalization of AuNP changes its transport behavior. Preliminary batch experiments suggested that BSA-cit-AuNP was much more stable than cit-AuNP. It was thus logical to expect BSA-cit-AuNP to be more stabilizing while flowing through a porous aqueous environment relative to weakly stabilized cit-AuNP. It was also logical to assume that Na^+ being a monovalent ion, would require a higher concentration to achieve the same level of destabilization Ca^{2+} would as Schulz-Hardy rule suggests. Both of these assumptions were proven to be at least partially inaccurate. It seemed that simple "rule of thumb" that are true for colloidal transport through porous media cannot be safely expected for coated-nanoparticles. BSA stabilizes AuNP through a combination of steric and electrostatic interaction, but the protein molecule itself mask the electro-repulsive property a gold nanoparticle possesses, leading to a weaker negative surface charge. In an environment where the surface charge of the porous media and the flowing particle were sufficiently neutralized, the electrosteric stabilizing effect of BSA could be overcome, as shown by some of the results from this project.

Another important point to note was the failure of the calculated attachment efficiency to describe the deposition behavior of AuNP. Attachment efficiency (α) along with the collector efficiency (η_0) have long been utilized by most studies examining nanoparticle transport through porous media. Yet it was demonstrated herein (as well as by Solovitch *et al.*) that α and η_0 fail to account for the most significant contributing factor of AuNP retention: aggregation and ripening.[42] Although these two parameters were very robust in other studies, caution should be taken as it was shown here that not

considering these processes may leave out important factors that affect nanoparticle transport.

Many important questions still await to be answered. While there were evidences suggesting that AuNP retention not accounted by α was due to aggregation and ripening, these evidences are circumstantial. For future work, it will be critical to investigate the morphology of the retained AuNP. The column used in this project was designed such that sections of the porous media can be removed independently for later analysis. TEM images of these sections would be invaluable to understand if aggregation and ripening had occurred significantly. The column outflow can also be connected to a DLS flow cell to observe weather the hydrodynamic diameter of the recovered AuNP changed. Another important factor to consider is AuNP size. For this project, only 15 nm AuNP were used. The literature has suggested that nanoparticle size can be a significant contributing factor affecting transport.[66] Future experiments should incorporate AuNP of different size, both smaller and larger, to compare and contrast transport and stability.

Appendix A – Nanoparticles and Porous Media Characterization

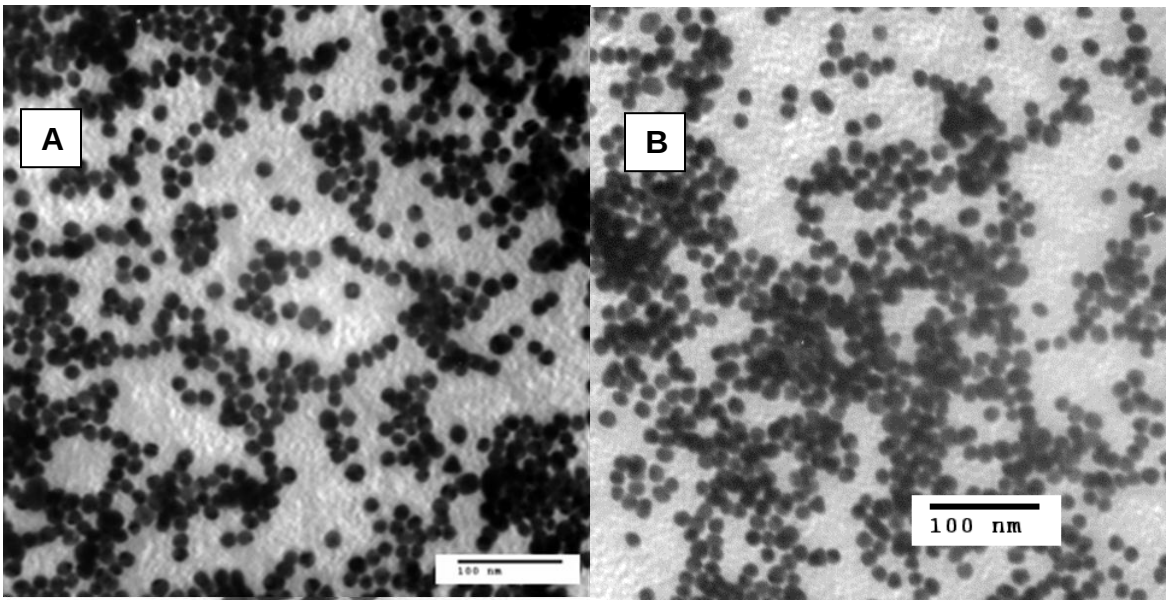

Figure S1 - TEM images of AuNP. A) Citrate-AuNP B) BSA-Citrate-AuNP. Size distribution for (A) is 15 ± 6.8 nm. Size distribution for (B) is 15 ± 6.8 nm. N = 619. PDI = 0.24.

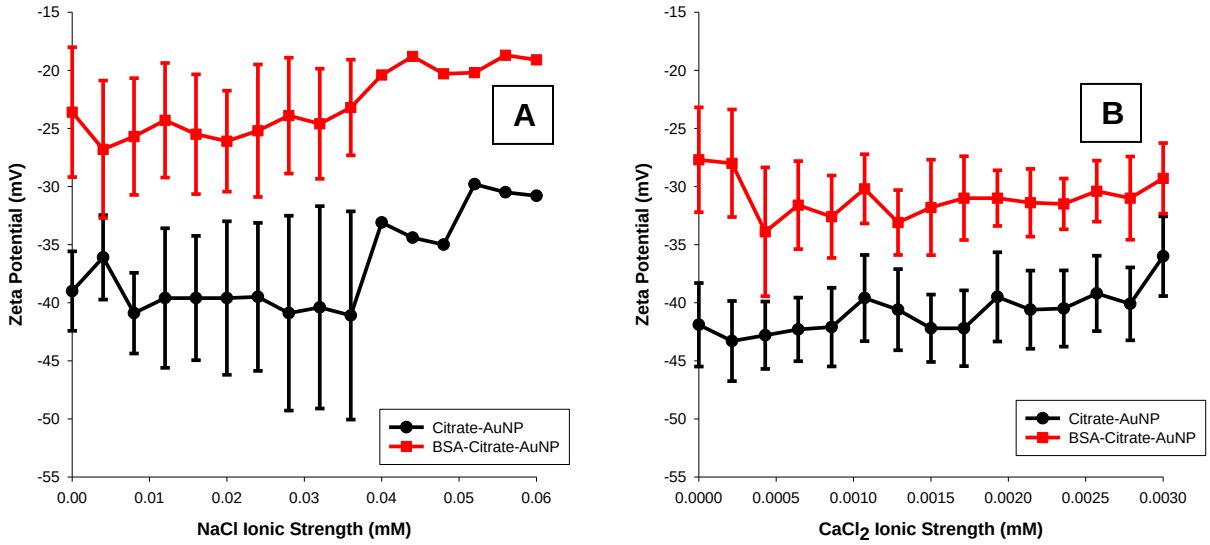

Figure S2 - AuNP zeta potential changes as ionic strength increases. pH was fixed at ≈8. A.) NaCl titration from 0 mM to 60 mM ionic strength. B.) $CaCl_2$ titration from 0 mM to 3 mM ionic strength. Error bars indicate 95% confidence interval; 20 measurements were collected per data point. Error bars missing in parts of plot A due to a loss of raw data by the instrument software.

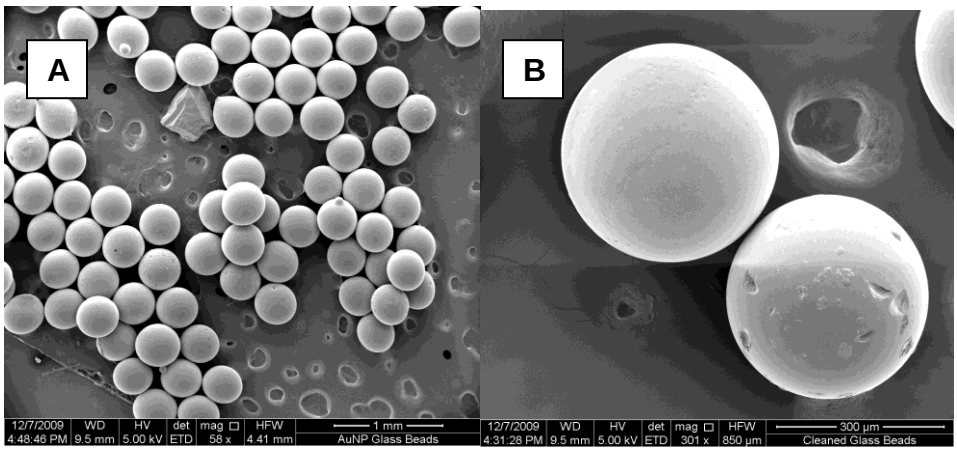

Figure S3 - SEM image of glass beads used for porous media in the packed column. A.) Glass beads provided by supplier "as is", prior to any cleaning. B.) Glass beads after vigorous cleaning process (as described in the methods section), the bead at the right has some mechanical blemishes

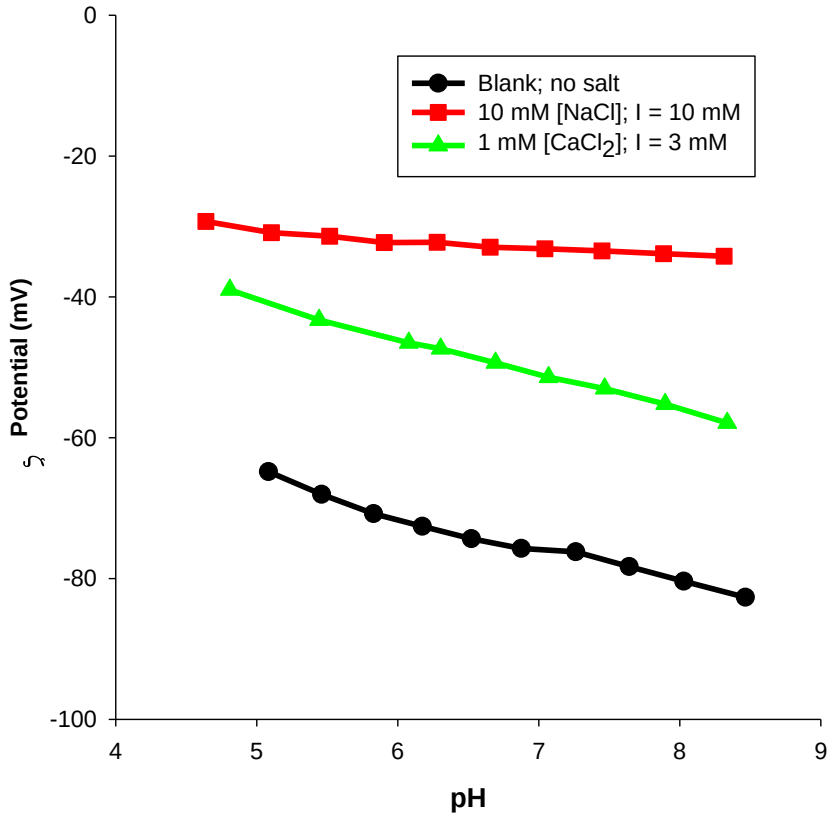

Figure S4 - Zeta potential of glass beads under different salt conditions.

Appendix B – Column Characterization

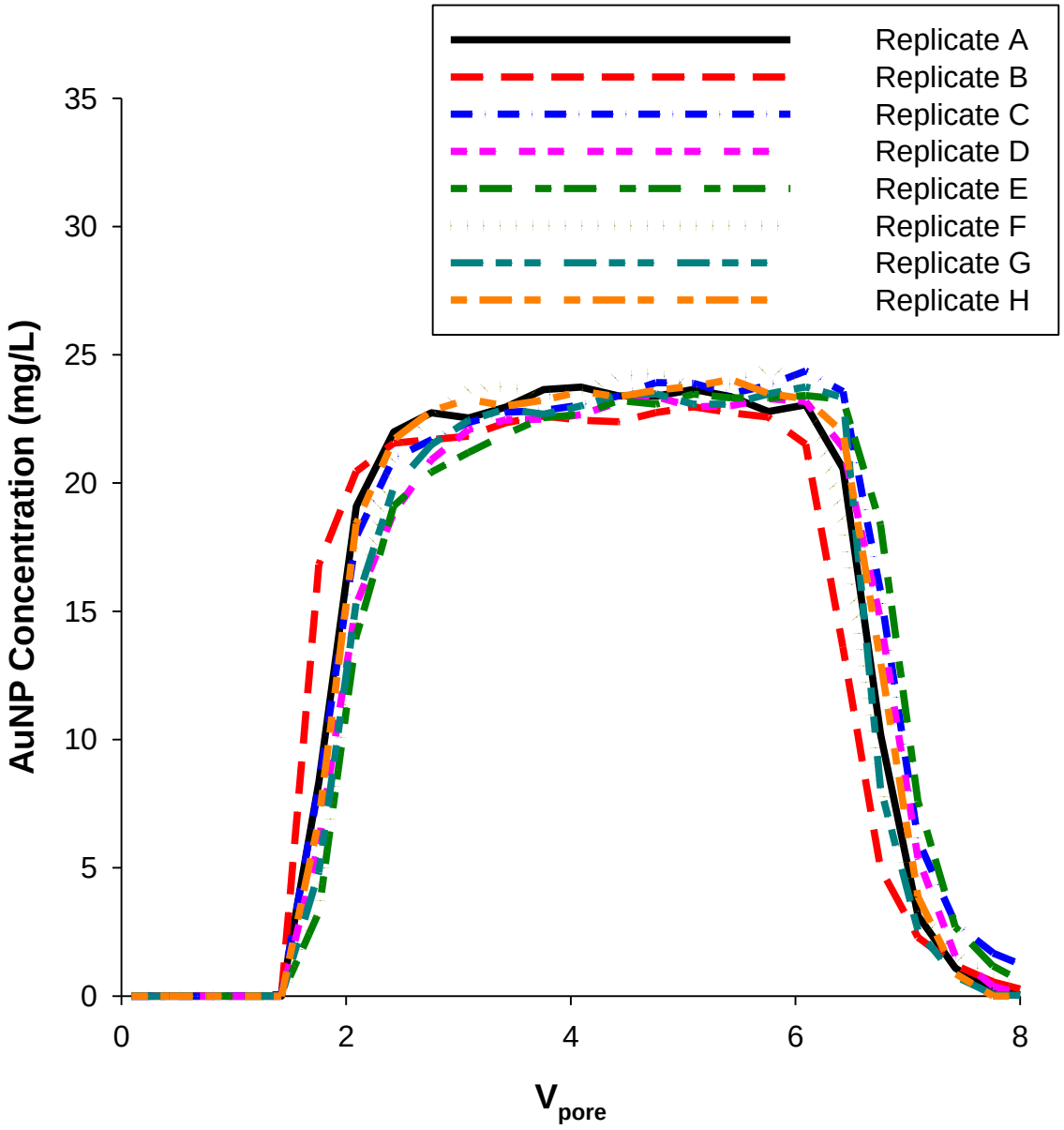

Figure S5 – Replicate Cit-AuNP breakthrough curves (n = 8). Diameter of citrate AuNP was 14 nm. Mobile phase onlly contained 2 mM $NaHCO_3$ as a buffer. C_0 for cit-AuNP was 24.5 mg/L. Injection volumn was $5V_{pore}$. Nitrate tracer performed before and after each replicate (data shown elsewhere).

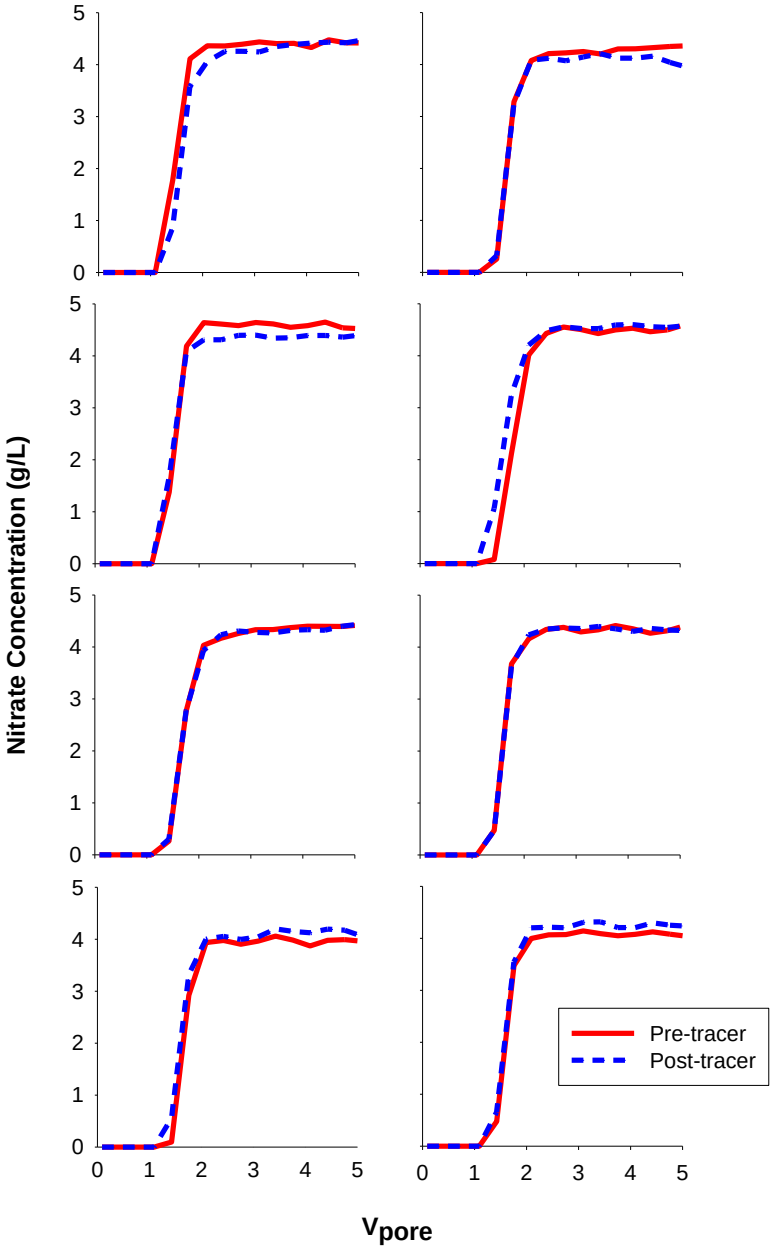

Figure S6 - Breakthrough curves from nitrate tracer that was performed before and after AuNP injection. C_0 for nitrate ($NaNO_3$) was 4.54 g/L. Injection volume was 5 V_{pore}. Mobile phase only contained 2 mM $NaHCO_3$ as a buffer. Each graph represents a pair of tracer breakthrough curves from an independent column experiment.

Appendix C - Evaluation of the affinity between collector media and AuNP

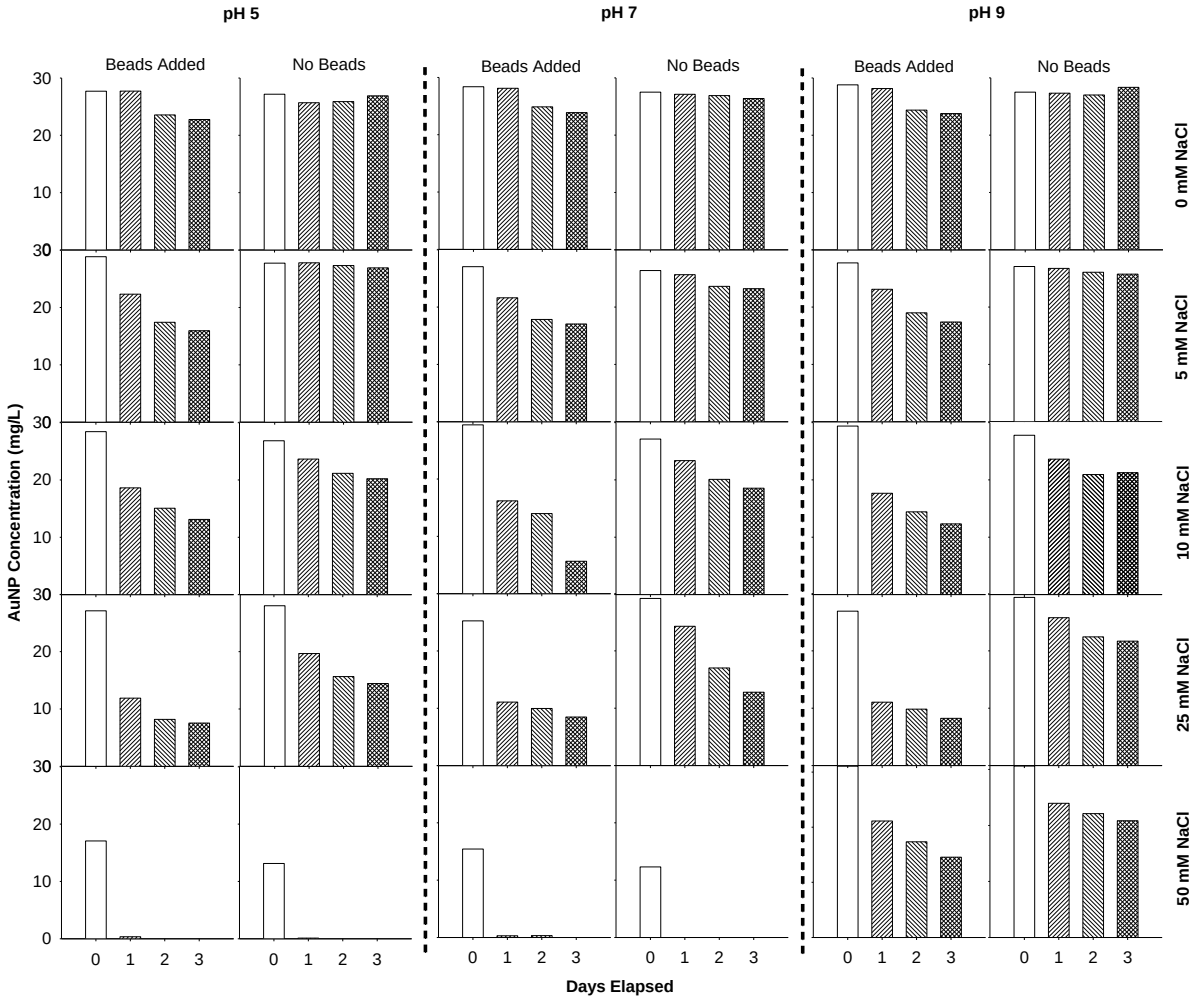

Figure S7 - Batch experiment results with NaCl and 14 mM citrate-AuNP, C_0 = 24.5 mg/L, mass of glass beads added to applicable rectors = 10 g.

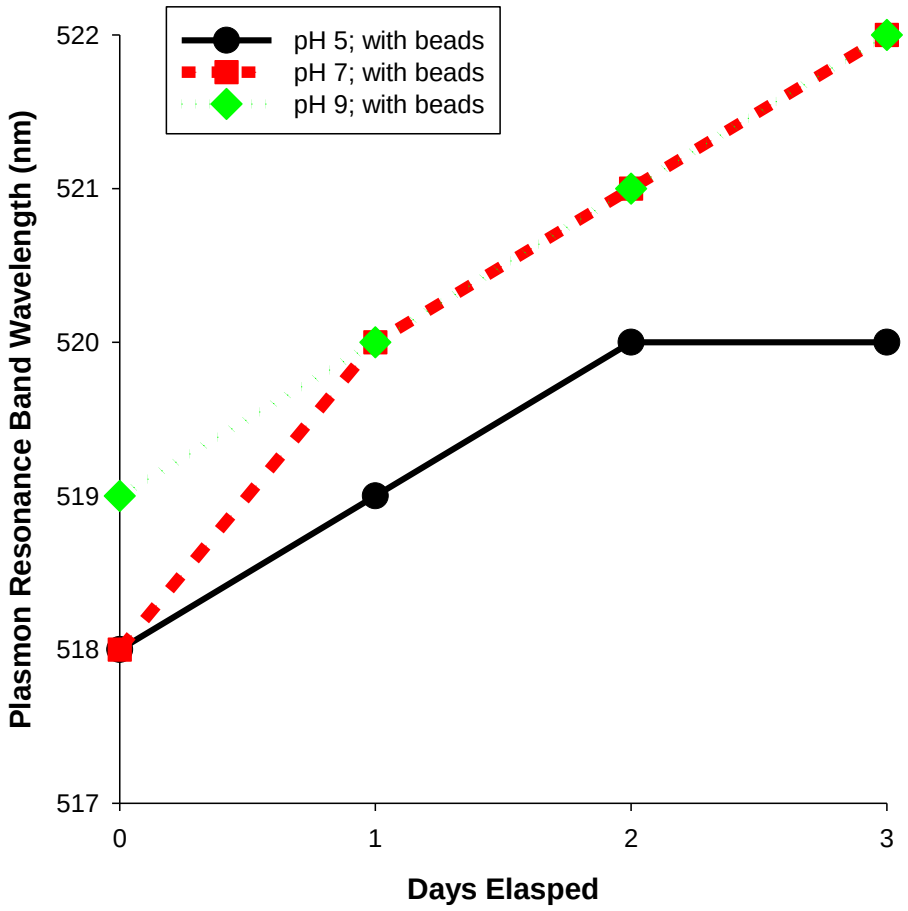

Figure S8 - Plasmon resonance band shift for selected batch reactors as time progresses. These data were from reactors that contained no NaCl, 2 mM $NaHCO_3$ as buffer, and pH as indicated in the legend. 24.5 mg/L of cit-AuNP spiked at day 0.

References

(1) Wiesner, M. R.; Lowry, G. V.; Alvarez, P.; Dionysiou, D.; Biswas, P. Assessing the Risks of Manufactured Nanomaterials. *Environ. Sci. Technol.* **2006**, *40*, 4336-4345.

(2) Woodrow Wilson International Center for Scholars - The Project on Emerging Nanotechonologies: Nanotechnology Consumer Product Inventory: Analysis http://www.nanotechproject.org/inventories/consumer/analysis_draft/ (accessed Apr 28, 2011).

(3) Bottero, J.-Y.; Wiesner, M. R. *Environmental nanotechnology: applications and impacts of nanomaterials*; McGraw-Hill Professional, 2007.

(4) Klaine, S. J.; Alvarez, P. J. J.; Batley, G. E.; Fernandes, T. F.; Handy, R. D.; Lyon, D. Y.; Mahendra, S.; McLaughlin, M. J.; Lead, J. R. Nanomaterials in the environment: Behavior, fate, bioavailability, and effects. *Environ. Toxicol. Chem.* **2008**, *27*, 1825-1851.

(5) Petosa, A. R.; Jaisi, D. P.; Quevedo, I. R.; Elimelech, M.; Tufenkji, N. Aggregation and Deposition of Engineered Nanomaterials in Aquatic Environments: Role of Physicochemical Interactions. *Environ. Sci. Technol.* **2010**, *44*, 6532-6549.

(6) Ghosh, P.; Han, G.; De, M.; Kim, C. K.; Rotello, V. M. Gold nanoparticles in delivery applications. *Adv. Drug Deliver. Rev.* **2008**, *60*, 1307-1315.

(7) Paciotti, G. F.; Kingston, D. G. I.; Tamarkin, L. Colloidal gold nanoparticles: a novel nanoparticle platform for developing multifunctional tumor-targeted drug delivery vectors. *Drug Develop. Res.* **2006**, *67*, 47-54.

(8) Paciotti, G. F.; Myer, L.; Weinreich, D.; Goia, D.; Pavel, N.; McLaughlin, R. E.; Tamarkin, L. Colloidal Gold: A Novel Nanoparticle Vector for Tumor Directed Drug Delivery. *Drug Deliv.* **2004**, *11*, 169-183.

(9) Visaria, R.; Bischof, J.; Loren, M.; Williams, B.; Ebbini, E.; Paciotti, G.; Griffin, R. Nanotherapeutics for enhancing thermal therapy of cancer. *Int. J. Hyperther.* **2007**, *23*, 501-511.

(10) Visaria, R. K.; Griffin, R. J.; Williams, B. W.; Ebbini, E. S.; Paciotti, G. F.; Song, C. W.; Bischof, J. C. Enhancement of tumor thermal therapy using gold nanoparticle–assisted tumor necrosis factor-α delivery. *Mol. Cancer Ther.* **2006**, *5*, 1014-1020.

(11) Brust, M.; Bethell, D.; Kiely, C. J.; Schiffrin, D. J. Self-Assembled Gold Nanoparticle Thin Films with Nonmetallic Optical and Electronic Properties. *Langmuir* **1998**, *14*, 5425-5429.

(12) Krasteva, N.; Besnard, I.; Guse, B.; Bauer, R. E.; Müllen, K.; Yasuda, A.; Vossmeyer, T. Self-Assembled Gold Nanoparticle/Dendrimer Composite Films for Vapor Sensing Applications. *Nano Lett.* **2002**, *2*, 551-555.

(13) Haruta, M. Gold as a novel catalyst in the 21st century: Preparation, working mechanism and applications. *Gold Bull.* **2004**, *37*, 27-36.

(14) Halvorson, R. A.; Vikesland, P. J. Surface-Enhanced Raman Spectroscopy (SERS) for Environmental Analyses. *Environ. Sci. Technol.* **2010**, *44*, 7749-7755.

(15) Mueller, N. C.; Nowack, B. Exposure Modeling of Engineered Nanoparticles in the Environment. *Environ. Sci. Technol.* **2008**, *42*, 4447-4453.

(16) Johnson, D. R.; Methner, M. M.; Kennedy, A. J.; Steevens, J. A. Potential for Occupational Exposure to Engineered Carbon-Based Nanomaterials in Environmental Laboratory Studies. *Environ. Health Persp.* **2009**.
(17) Ferry, J. L.; Craig, P.; Hexel, C.; Sisco, P.; Frey, R.; Pennington, P. L.; Fulton, M. H.; Scott, I. G.; Decho, A. W.; Kashiwada, S.; Murphy, C. J.; Shaw, T. J. Transfer of gold nanoparticles from the water column to the estuarine food web. *Nat. Nanotechonol.* **2009**, *4*, 441-444.
(18) Judy, J. D.; Unrine, J. M.; Bertsch, P. M. Evidence for Biomagnification of Gold Nanoparticles within a Terrestrial Food Chain. *Environ. Sci. Technol.*
(19) Khan, J. A.; Pillai, B.; Das, T. K.; Singh, Y.; Maiti, S. Molecular Effects of Uptake of Gold Nanoparticles in HeLa Cells. *ChemBioChem* **2007**, *8*, 1237-1240.
(20) Pan, Y.; Neuss, S.; Leifert, A.; Fischler, M.; Wen, F.; Simon, U.; Schmid, G.; Brandau, W.; Jahnen-Dechent, W. Size-Dependent Cytotoxicity of Gold Nanoparticles. *Small* **2007**, *3*, 1941-1949.
(21) Robertson, W. D.; Barker, J. F.; LeBeau, Y.; Marcoux, S. Contamination of an Unconfined Sand Aquifer by Waste Pulp Liquor: A Case Study. *Ground Water* **1984**, *22*, 191-197.
(22) McCarthy, J.; Zachara, J. Subsurface Transport of Contaminants - Mobile Colloids in the Subsurface Environment May Alter the Transport of Contaminants. *Environ. Sci. Technol.* **1989**, *23*, 496-502.
(23) Sauerbrey, G. The Use of Quartz Crystal Oscillators for Weighing Thin Layers and for Microweighing Applications. *Z. Phys. A-Hadron. Nucl.* **1959**, *155*, 206-222.
(24) Bruckenstein, S.; Shay, M. Experimental aspects of use of the quartz crystal microbalance in solution. *Electrochim. A* **1985**, *30*, 1295-1300.
(25) da Silva, A. K.; Kavanagh, O. V.; Estes, M. K.; Elimelech, M. Adsorption and Aggregation Properties of Norovirus GI and GII Virus-like Particles Demonstrate Differing Responses to Solution Chemistry. *Environ. Sci. Technol.*
(26) Guzman, K. A. D.; Finnegan, M. P.; Banfield, J. F. Influence of Surface Potential on Aggregation and Transport of Titania Nanoparticles. *Environ. Sci. Technol.* **2006**, *40*, 7688-7693.
(27) Yao, K.-M.; Habibian, M. T.; O'Melia, C. R. Water and waste water filtration. Concepts and applications. *Environ. Sci. Technol.* **1971**, *5*, 1105-1112.
(28) Tufenkji, N.; Elimelech, M. Correlation Equation for Predicting Single-Collector Efficiency in Physicochemical Filtration in Saturated Porous Media. *Environ. Sci. Technol.* **2004**, *38*, 529-536.
(29) Lecoanet, H. F.; Bottero, J.-Y.; Wiesner, M. R. Laboratory Assessment of the Mobility of Nanomaterials in Porous Media. *Environ. Sci. Technol.* **2004**, *38*, 5164-5169.
(30) Derjaguin, B. V.; Landau, L. Theory of the stability of strongly charged lyophobic sols and the adhesion of strongly charged particles in solutions of electrolytes. *Acta Physicochim. USSR* **1941**, *14*, 633-662.
(31) Verwey, E. J. .; Overbeek, J. T. . *Theory of the stability of lyophobic colloids: the interaction of sol particles having an electric double layer*; Elsevier New York, 1948.

(32) Lecoanet, H. F.; Wiesner, M. R. Velocity Effects on Fullerene and Oxide Nanoparticle Deposition in Porous Media. *Environ. Sci. Technol.* **2004**, *38*, 4377-4382.
(33) Espinasse, B.; Hotze, E. M.; Wiesner, M. R. Transport and Retention of Colloidal Aggregates of C60 in Porous Media: Effects of Organic Macromolecules, Ionic Composition, and Preparation Method. *Environ. Sci. Technol.* **2007**, *41*, 7396-7402.
(34) Wang, Y.; Li, Y.; Fortner, J. D.; Hughes, J. B.; Abriola, L. M.; Pennell, K. D. Transport and Retention of Nanoscale C60 Aggregates in Water-Saturated Porous Media. *Environ. Sci. Technol.* **2008**, *42*, 3588-3594.
(35) Li, Y.; Wang, Y.; Pennell, K. D.; Abriola, L. M. Investigation of the Transport and Deposition of Fullerene (C60) Nanoparticles in Quartz Sands under Varying Flow Conditions. *Environ. Sci. Technol.* **2008**, *42*, 7174-7180.
(36) Franchi, A.; O'Melia, C. R. Effects of Natural Organic Matter and Solution Chemistry on the Deposition and Reentrainment of Colloids in Porous Media. *Environ. Sci. Technol.* **2003**, *37*, 1122-1129.
(37) Tufenkji, N.; Elimelech, M. Breakdown of Colloid Filtration Theory: Role of the Secondary Energy Minimum and Surface Charge Heterogeneities. *Langmuir* **2005**, *21*, 841-852.
(38) Pelley, A. J.; Tufenkji, N. Effect of particle size and natural organic matter on the migration of nano- and microscale latex particles in saturated porous media. *J. Colloid Interf. Sci.* **2008**, *321*, 74-83.
(39) Saleh, N.; Kim, H.-J.; Phenrat, T.; Matyjaszewski, K.; Tilton, R. D.; Lowry, G. V. Ionic Strength and Composition Affect the Mobility of Surface-Modified Fe0 Nanoparticles in Water-Saturated Sand Columns. *Environ. Sci. Technol.* **2008**, *42*, 3349-3355.
(40) Jaisi, D. P.; Saleh, N. B.; Blake, R. E.; Elimelech, M. Transport of Single-Walled Carbon Nanotubes in Porous Media: Filtration Mechanisms and Reversibility. *Environ. Sci. Technol.* **2008**, *42*, 8317-8323.
(41) Jaisi, D. P.; Elimelech, M. Single-Walled Carbon Nanotubes Exhibit Limited Transport in Soil Columns. *Environ. Toxicol. Chem.* **2009**, *43*, 9161-9166.
(42) Solovitch, N.; Labille, J.; Rose, J.; Chaurand, P.; Borschneck, D.; Wiesner, M. R.; Bottero, J.-Y. Concurrent Aggregation and Deposition of TiO2 Nanoparticles in a Sandy Porous Media. *Environ. Sci. Technol.* **2010**, *44*, 4897-4902.
(43) Turkevich, J.; Stevenson, P. C.; Hillier, J. A study of the nucleation and growth processes in the synthesis of colloidal gold. *Discuss. Faraday Soc.* **1951**, *11*.
(44) Brewer, S. H.; Glomm, W. R.; Johnson, M. C.; Knag, M. K.; Franzen, S. Probing BSA Binding to Citrate-Coated Gold Nanoparticles and Surfaces. *Langmuir* **2005**, *21*, 9303-9307.
(45) Saleh, N. B.; Pfefferle, L. D.; Elimelech, M. Influence of Biomacromolecules and Humic Acid on the Aggregation Kinetics of Single-Walled Carbon Nanotubes. *Environ. Sci. Technol.* **2010**, *44*, 2412-2418.
(46) Tufenkji, N.; Miller, G. F.; Ryan, J. N.; Harvey, R. W.; Elimelech, M. Transport of Cryptosporidium Oocysts in Porous Media: Role of Straining and Physicochemical Filtration†. *Environ. Sci. Technol.* **2004**, *38*, 5932-5938.

(47) Delgado, A. V.; González-Caballero, F.; Hunter, R. J.; Koopal, L. K.; Lyklema, J. Measurement and interpretation of electrokinetic phenomena. *J. Colloid Interf. Sci.* **2007**, *309*, 194-224.
(48) Ji, X.; Song, X.; Li, J.; Bai, Y.; Yang, W.; Peng, X. Size Control of Gold Nanocrystals in Citrate Reduction: The Third Role of Citrate. *J. Am. Chem. Soc* **2007**, *129*, 13939-13948.
(49) Ao, L.; Gao, F.; Pan, B.; Cui, D.; Gu, H. Interaction between Gold Nanoparticles and Bovine Serum Albumin or Sheep Antirabbit Immunoglobulin G. *Chin. J. Chem.* **2006**, *24*, 253-256.
(50) Eaton, A. D.; Clesceri, L. S.; Rice, E. W.; Greenberg, A. E.; Franson, M. A. H. *Standard Methods for the Examination of Water & Wastewater: Centennial Edition*; 21st ed.; Amer Public Health Assn, 2005.
(51) Smoluchowski, M. Contributiona la théorie de l'endosmose électrique et de quelques phenomenes corrélatifs. *Bull. Intl Acad. Sci. Cracovie* **1903**, *8*, 182–200.
(52) Rezwan, K.; Studart, A. R.; Vörös, J.; Gauckler, L. J. Change of ζ Potential of Biocompatible Colloidal Oxide Particles upon Adsorption of Bovine Serum Albumin and Lysozyme. *J. Phys. Chem. B* **2005**, *109*, 14469-14474.
(53) Rezwan, K.; Meier, L. P.; Rezwan, M.; Vörös, J.; Textor, M.; Gauckler, L. J. Bovine Serum Albumin Adsorption onto Colloidal Al2O3 Particles: A New Model Based on Zeta Potential and UV−Vis Measurements. *Langmuir* **2004**, *20*, 10055-10061.
(54) Hardy, W. B. A preliminary investigation of the conditions which determine the stability of irreversible hydrosols. *P. R. Soc. London* **1900**, *66*, 110-125.
(55) Schulze, H. Schwefelarsen in wässriger Lösung. *J. Prakt. Chem.* **1882**, *25*, 431-452.
(56) Elimelech, M.; O'Melia, C. R. Kinetics of deposition of colloidal particles in porous media. *Environ. Sci. Technol.* **1990**, *24*, 1528-1536.
(57) Diegoli, S.; Manciulea, A.; Begum, S.; Jones, I.; Lead, J.; Preece, J. Interaction between manufactured gold nanoparticles and naturally occurring organic macromolecules. *Sci. Total Environ.* **2008**, *402*, 51-61.
(58) Khlebtsov, N.; Dykman, L.; Krasnov, Y.; Mel'nikov, A. Light absorption by the clusters of colloidal gold and silver particles formed during slow and fast aggregation. *Colloid J+* **2000**, *62*, 765-779.
(59) Elimelech, M. Effect of Particle Size on the Kinetics of Particle Deposition under Attractive Double Layer Interactions. *J. Colloid Interf. Sci.* **1994**, *164*, 190-199.
(60) Bergström, L. Hamaker constants of inorganic materials. *Adv. Colloid Interfac.* **1997**, *70*, 125-169.
(61) Liu, X.; Wazne, M.; Christodoulatos, C.; Jasinkiewicz, K. L. Aggregation and deposition behavior of boron nanoparticles in porous media. *J. Colloid Interf. Sci.* **2009**, *330*, 90-96.
(62) Israelachvili, J. N. *Intermolecular and Surface Forces*; 3rd ed.; Academic Press: Burlington, MA, 2011.
(63) van Oss, C. J. *Interfacial Forces in Aqueous Media, Second Edition*; 2nd ed.; CRC Press, 2006.
(64) Hunter, R. J. *Foundations of Colloid Science*; 2nd ed.; Oxford University Press: Oxford, 2001.

(65) Hogg, R.; Healy, T. W.; Fuerstenau, D. W. Mutual coagulation of colloidal dispersions. *T. Faraday Soc.* **1966**, *62*, 1638.
(66) Zhang, W.; Rittmann, B.; Chen, Y. Size Effects on Adsorption of Hematite Nanoparticles on E. coli cells. *Environ. Sci. Technol.*